TU Delft

Delft University of Technology

Document Version
Final published version

Licence
CC BY

Citation (APA)
Baluchová, S., & Buijnsters, J. G. (2025). Diamond 2D/3D Printing Technology: Bringing Scintillating Performance to Functional Materials and Their Applications. *Advanced Materials Technologies*, *10*(22), Article e01111. https://doi.org/10.1002/admt.202501111

Important note
To cite this publication, please use the final published version (if applicable).
Please check the document version above.

Copyright
In case the licence states “Dutch Copyright Act (Article 25fa)”, this publication was made available Green Open Access via the TU Delft Institutional Repository pursuant to Dutch Copyright Act (Article 25fa, the Taverne amendment). This provision does not affect copyright ownership.
Unless copyright is transferred by contract or statute, it remains with the copyright holder.

Sharing and reuse
Other than for strictly personal use, it is not permitted to download, forward or distribute the text or part of it, without the consent of the author(s) and/or copyright holder(s), unless the work is under an open content license such as Creative Commons.

Takedown policy
Please contact us and provide details if you believe this document breaches copyrights.
We will remove access to the work immediately and investigate your claim.

This work is downloaded from Delft University of Technology.

Check for updates

ADVANCED MATERIALS TECHNOLOGIES
www.advmattechnol.de

Diamond 2D/3D Printing Technology: Bringing Scintillating Performance to Functional Materials and Their Applications

Simona Baluchová and Josephus G. Buijnsters**

Diamond's unique combination of hardness, high thermal conductivity, chemical inertness, and biocompatibility makes it a highly attractive material for next-generation technologies. However, its integration into functional devices has long been limited by the difficulties of processing bulk diamond. Recent advances in additive manufacturing have enabled the use of diamond in nano- and microparticulate forms, significantly expanding its accessibility and versatility. This review presents the state-of-the-art in printing with diamond particles using inkjet, screen, microcontact, and 3D printing techniques, which offer enhanced design freedom, compatibility with diverse substrates, and streamlined prototyping workflows. Particular emphasis is placed on how particle properties, together with ink, resin, filament, or powder formulation, influence print quality and final performance. The reviewed applications span microfabricated structures, various sensing, and thermal management devices, wear-resistant tools, and biomedical interfaces. Key technical challenges, including particle dispersion, interfacial bonding, and equipment wear, are addressed alongside emerging strategies such as surface functionalization, AI-assisted process optimization, and multimaterial integration. By bridging materials science and device engineering, printed diamond technologies offer a scalable and flexible route to high-performance, multifunctional components. This review serves as a resource for researchers aiming to integrate diamond into advanced printed material platforms.

1. Introduction

Diamond exhibits an extraordinary combination of properties, including extreme hardness, high thermal conductivity, chemical inertness, and biocompatibility,[1,2] that make it uniquely attractive for a wide range of applications, from electronics and quantum technologies to sensing, biomedical interfaces, and thermal management.[3–5] However, the integration of diamond into device architectures has historically been constrained by the limitations of conventional fabrication techniques. The exceptional mechanical hardness and chemical inertness of diamond, while beneficial in application, make traditional subtractive processes such as etching[6] and micromachining[7] labor-intensive, expensive, and poorly suited for creating fine or complex features. As modern technologies continue to evolve toward greater complexity, miniaturization, and flexibility, there is a growing demand for alternative fabrication strategies that can unlock diamond's full potential in advanced functional devices.

In addition to bulk single-crystal[8,9] or polycrystalline diamond (films),[3,10] which have traditionally dominated most applications, diamond is also available in particulate forms; namely, nanodiamonds (NDs)[11–13] and microdiamond powders.[14] These particles preserve diamond's intrinsic properties, such as chemical inertness, biocompatibility, and exceptional thermal conductivity, while offering greater processability and versatility. Their small size and dispersibility in various media make them particularly suitable for integration into additive manufacturing processes. When formulated into printable inks, resins, filaments, or powder mixtures, diamond particles enable the fabrication of complex, functional structures that would be difficult or impractical to realize with bulk diamond alone. Moreover, these diamond particles can be either intrinsic (undoped), suitable for structural, thermal, or optical uses, or boron-doped[15] when electrical conductivity is required, for example, in electrochemical sensors.[16–18] Commercial availability of both intrinsic and boron-doped diamond (BDD) particles has further facilitated their adoption across a growing number of research and industrial domains.

S. Baluchová
Department of Analytical Chemistry
Faculty of Science
Charles University
Albertov 6, Prague 2 128 00, Czech Republic
E-mail: simona.baluchova@natur.cuni.cz

J. G. Buijnsters
Department of Precision and Microsystems Engineering
Faculty of Mechanical Engineering
Delft University of Technology
Mekelweg 2, Delft 2628 CD, The Netherlands
E-mail: j.g.buijnsters@tudelft.nl

The ORCID identification number(s) for the author(s) of this article can be found under https://doi.org/10.1002/admt.202501111

© 2025 The Author(s). Advanced Materials Technologies published by Wiley-VCH GmbH. This is an open access article under the terms of the Creative Commons Attribution License, which permits use, distribution and reproduction in any medium, provided the original work is properly cited.

DOI: 10.1002/admt.202501111

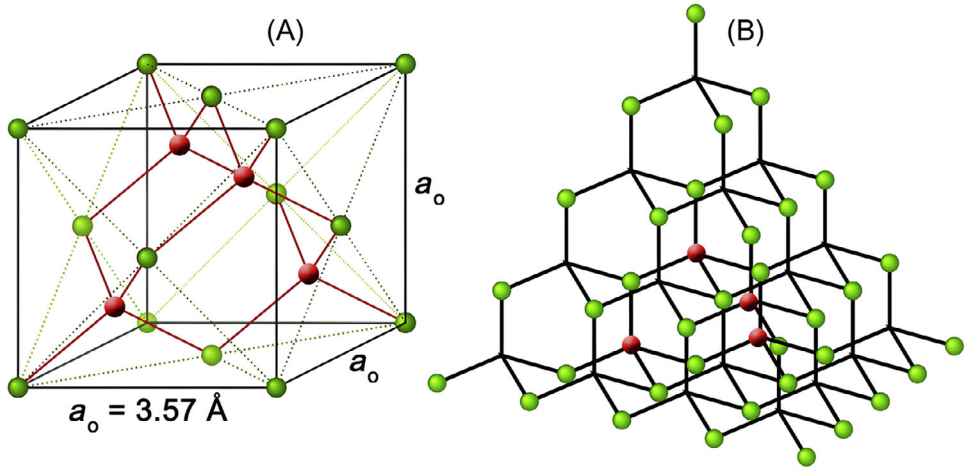


Figure 1. A) Schematic of the diamond crystal unit cell, illustrating the cubic lattice arrangement. B) Tetrahedral bonding structure of diamond, where each carbon atom is covalently bonded to four nearest neighbors. Colors are used solely for clarity; all atoms are carbon. Red-colored atoms indicate carbon atoms positioned within the unit cell. Reproduced with permission from ref. [24]. Copyright 2019, Elsevier.

Building on this material accessibility, the rapid development of printing technologies, particularly various 3D printing techniques, has opened new possibilities for the integration of diamond nano- and microparticles into functional materials and devices. Additive manufacturing allows for direct, layer-by-layer construction of complex geometries with minimal material waste, maskless patterning, and compatibility with a broad range of substrates, including flexible and stretchable ones.[19–21] These methods offer significant advantages in research contexts: prototyping is faster, cleaner, and more accessible than conventional lithography-based fabrication, enabling rapid exploration of new architectures with only a few samples and reduced dependence on cleanroom environments.

Importantly, these developments overlap with a dramatic reduction in the price of synthetic diamond,[22] including its particulate forms. As a result, diamond is no longer an exotic or prohibitively expensive material, but one increasingly viable for wider use in research and industry.

In fact, in his 2018 outlook on the future of carbon science, Ruoff identified the creation of novel diamond shapes, including 3D-printed structures, as a key research goal for the coming years.[23] Several years on, this prediction has proven visionary: as this review shows, printing with diamond particles has evolved into a dynamic area of materials research, enabling structures and functionalities not easily attainable with conventional fabrication approaches.

This review provides a comprehensive overview of the state-of-the-art in printing with (doped) diamond nano- and microparticles. Section 2 outlines the material science of diamond particles, including their structure, properties, synthesis, and surface functionalization. Section 3 details the printing techniques used to process them, ranging from screen, inkjet, and microcontact printing to modern 3D printing-based approaches. Section 4 highlights emerging applications, including patterned and/or miniaturized diamond microstructures, sensors, thermal interfaces, machining tools, biomedical implants, optics, and quantum technologies. We conclude with a perspective on current challenges and opportunities for advancing printed diamond technologies.

2. Diamond Particles

2.1. Diamond Structure and Material Properties

Diamond is an allotropic form of carbon with its atoms arranged in a crystal lattice structure. Each carbon atom shares electrons and forms single covalent bonds with four neighboring carbon atoms, resulting in a densely packed tetrahedral arrangement (**Figure 1**). The diamond structure has the highest atomic number density among all materials (i.e., 1.76×10^{23} atoms cm^{-3}) and accounts for the unique combination of properties that make diamond one of the most versatile materials in the world.

Diamond's extreme properties, such as the widest electromagnetic transmission spectrum, chemical robustness, and highest hardness and thermal conductivity, are ideally suited for major industrial applications including diffractive optics,[25] machining tools,[26] abrasives,[27] water treatment anodes,[10,28] electronics,[29] and sensors.[30] Some principal properties of (bulk) diamond are listed in **Table 1** (left column). From this summary, it is evident that diamond holds great potential for realizing advanced solutions in the various mechanical, chemical, biomedical, optical, and electrical engineering disciplines. Small-sized diamonds (e.g., detonation-derived diamond nanoparticles) may present divergent assets by virtue of their high surface-to-volume ratio (Table 1, right column), and their applications result from either the bulk diamond core, surface interactions, or a combination of both.[31]

2.2. Synthesis and Particle Structure

The intrinsic variability and scarcity of natural diamonds limit their use in engineering applications. However, owing to the major advances in synthesis techniques over the past few decades,

© 2025 The Author(s). Advanced Materials Technologies published by Wiley-VCH GmbH

2365709x, 2025, 22, Downloaded from https://advanced.onlinelibrary.wiley.com/doi/10.1002/admt.202501111, Wiley Online Library on [19/11/2025]. See the Terms and Conditions (https://onlinelibrary.wiley.com/terms-and-conditions) on Wiley Online Library for rules of use; OA articles are governed by the applicable Creative Commons License

Table 1. Selected material properties of (bulk) diamond[1,2] and specific characteristics of detonation nanodiamonds (DNDs).[31]

Material properties of [bulk] diamond	Specific characteristics of DNDs	
Hardest bulk material (Vickers hardness 70–150 GPa)	Size of primary particles ≈4–6 nm	
High wear resistance and stable low self-mating friction (0.02–0.1)	Quasi-spherical shape	
Broad optical transparency from UV (225 nm) to far IR	Core	Mechanical/chemical stability
Highest thermal conductivity at room temperature (2000 W m^{-1} K^{-1})		High thermal conductivity
Low thermal expansion coefficient (1.1 ppm K^{-1})		High transparency; UV scattering
Highest known resistance to thermal shock (30 000 kW m^{-1})	Surface	Colloidal stability
Wide-bandgap semiconductor (band gap 5.5 eV)		Uniform distribution in composites
Can be doped (e.g., with B) and gain metal-like electrical conductivity		Electron affinity (e.g., negative)
High dielectric strength (10 000 kV cm^{-1})		Catalytic properties
Very resistant to chemical corrosion		Drug adsorption
High biocompatibility		Conjugation with biomolecules

it is now possible to produce consistently designed synthetic diamond in a wide variety of forms ranging from particles of only a few nanometers to bulk crystals up to cm size.[32] Diamond particles finer than ≈100 microns are increasingly utilized in printing and are generally referred to as diamond powder. In terms of its particle size, diamond powder belongs to either micron, submicron, or nano powder.

Diamond micropowder is widely used for grinding and polishing various hard materials, and it plays a role in many high-tech industries.[33,34] The most common varieties are diamond micropowders produced from low-strength synthetic diamonds through milling or crushing, purification, and particle size grading.[35] Air-flow grinding and/or mechanical ball milling are used for the fragmentation and shaping of the diamond powders. By sintering diamond micropowders and then grinding them, diamond polycrystalline powders are created; they find their use in the production of monocrystalline diamond tools, boring tools, tools for the building industry, and concrete and stone grinding.

Regarding NDs, a range of static and dynamic production methods have been invented. The "top-down" crushing of microcrystals grown at static high-pressure high-temperature (HPHT)[36] and the detonation of carbon-containing explosives (e.g., mixture of trinitrotoluene and hexogen) as a "bottom-up" approach,[37] respectively, are the most widely applied techniques for commercial purposes. Other methods include, among others, laser ablation,[38] chemical vapor deposition,[39] ion irradiation of graphite,[40] and ultrasound cavitation.[41]

The large-scale production of detonation nanodiamonds (DNDs) and HPHT nanodiamonds (HPHT NDs) (**Figure 2**) makes them readily available. However, the behavior of the NDs can vary dramatically between suppliers, and a large part of the variability in the material stems from its production and processing history. Notably, the DNDs and HPHT NDs have distinct morphological features. As-produced DNDs form tight inseparable aggregates of primary particles,[42] but disaggregation by milling (bead/jet) promotes the creation of colloidally stable dispersions of primary DND particles (Figure 2D) with quasi-spherical shape (≈4–6 nm in diameter) in a wide range of solvents.[31] HPHT NDs typically exhibit irregular shapes with sharp facets (Figure 2C) and are available with the smallest average particle size ≈10–20 nm, although rounded sub-10 nm particles of HPHT diamond have been obtained occasionally.[31] The impurity content of DNDs is typically much higher than that of HPHT NDs. "Detonation soot", the raw product of detonation synthesis, contains a large amount of graphitic (sp^2) carbon (up to ≈70 wt.%) and incombustible inorganic impurities such as metals and metal oxides (1–8 wt.%).[43] Consequently, purification of DNDs combining mechanical (e.g., colloidal grinding), thermal (e.g., heating in air or hydrogen atmosphere), and/or chemical (e.g., wet oxidation, acid dissolution) methods is widespread. The primary goal of most of these gas/liquid-phase approaches is the removal of non-diamond carbon phases that are present on the surfaces of HPHT diamonds and aggregates of DNDs. Also, the use of these techniques can lead to disaggregation, size reduction, and the removal of metallic impurities, which can conjugate the primary particles.[43] Generally, obtaining a single, narrow-size distribution of NDs is very challenging. Thus, some form of fractionation is required. This is typically achieved by dispersing the NDs within a solvent using ultrasonic cavitation, followed by centrifugation to reach selected particle size fractions.[44]

Resolving the complexity of underlying nanodiamond structures and the controversies surrounding their polymorphic forms is a highly challenging task.[45] Octahedral, truncated octahedral, cuboctahedral, and cuboid shapes, consisting of (100) and (111) facets, have been reported.[46] Considering the core of diamond particles, DNDs often contain twin and multiple twin defects,[47] while nitrogen is the most common impurity/dopant.[48] Defect complexes of vacancies trapped by nitrogen atoms form different color centers, which, in particular, have generated immense research interest from the biomedical and life sciences, quantum technology, and optics communities in recent years.[49–52] The surface structure of ND particles is determined by their size, shape, and surface functionalization.[53]

Bulk diamond is a wide bandgap semiconductor, but heavily BDD with metallic type conductivity (boron content > 10^{20} cm^{-3}) is acknowledged as one of the best electrode materials for electrochemical purposes. BDD micro- and nano-powders are therefore a popular material choice in the manufacturing of advanced sensors (see Subsection 4.2.2). Both surface and bulk-doped diamond powders are applied, yet the commercial availability of the BDD powders is very limited. Using CVD, the coating of insulating diamond powders by a (thin) boron-doped layer produces core-shell particles with high surface conductivity.[14,15]

© 2025 The Author(s). Advanced Materials Technologies published by Wiley-VCH GmbH

2365709x, 2025, 22, Downloaded from https://advanced.onlinelibrary.wiley.com/doi/10.1002/admt.202501111, Wiley Online Library on [19/11/2025]. See the Terms and Conditions (https://onlinelibrary.wiley.com/terms-and-conditions) on Wiley Online Library for rules of use; OA articles are governed by the applicable Creative Commons License

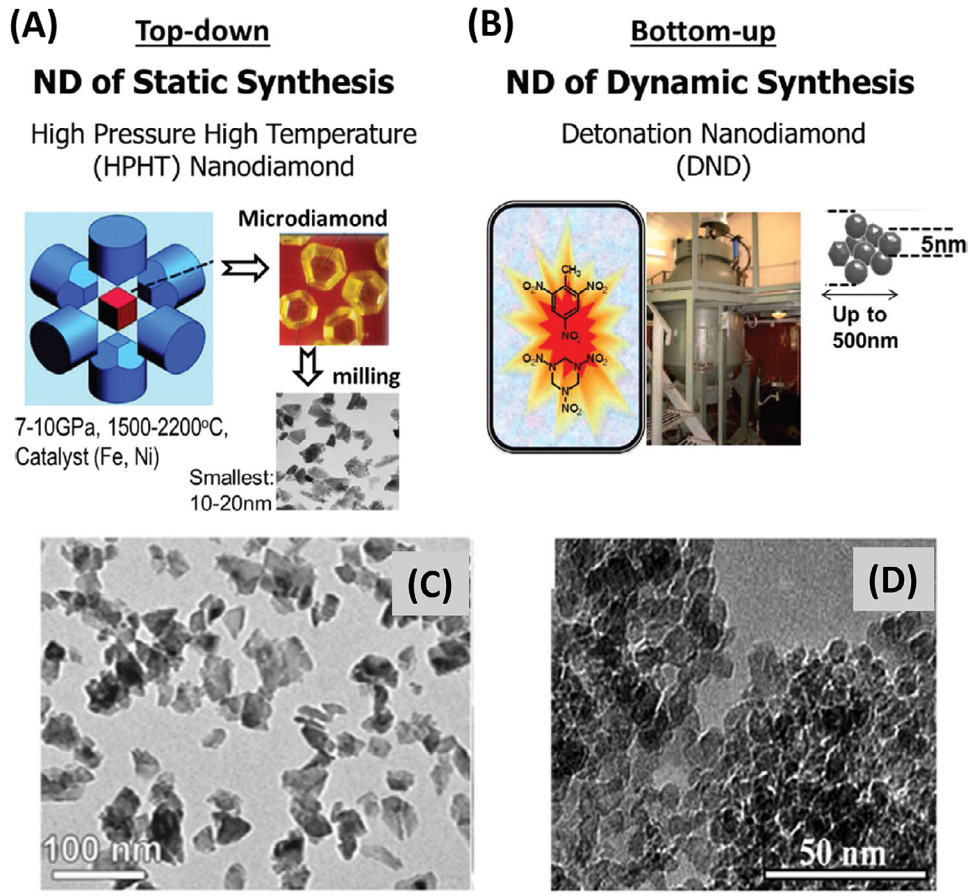


Figure 2. Schematic representation of the synthesis and structure of the two major types of nanodiamond particles: A) "top-down" production of NDs by mechanical size reduction of microdiamond powders manufactured by static high-pressure, high-temperature (HPHT) synthesis, and B) "bottom-up" production of DNDs by detonation of carbon-containing explosives. Reproduced with permission from ref. [53]. Copyright 2015, AIP Publishing. Transmission electron microscopy (TEM) images of batches of C) HPHT NDs and D) DNDs. Reproduced with permission from ref. [55]. Copyright 2017, Elsevier.

Bulk-doped BDD powders are typically produced by crushing polycrystalline BDD (thick) films[54] or through tailored HPHT synthesis.

2.3. Surface Functionalization and Application

This review article does not have the intention to provide a comprehensive overview of the different methodologies of synthesis, purification, and surface functionalization of diamond powders, nor does it cover the full range of reported scientific and industrial applications that exploit these materials. Its main objective is to survey the printing of diamond particles and the emerging advanced composites, system components, devices, and tools that have been print-manufactured with diamond powders to date. For a more detailed discussion of the theory and practice of the synthesis and purification of NDs and the in-depth examination of surface functionalization and application domains of NDs, the reader is referred to.[11–13,31,56–58]

In short, the graphitization of the (111) diamond facet,[53] a shape-dependent surface instability, leads characteristically to inherent changes in surface hybridization, reactivity, and electrostatic potential and thus impacts the interaction of NDs and their surroundings and surfactants.[46] Over a wide size range, NDs terminated with atomic hydrogen and oxygen and hydroxyl functional groups are reported. After purification from sp^2 carbon by oxidation (e.g., acid cleaning), the surface of detonation NDs contains a complex mixture of oxygen-rich surface groups, including carboxylic acids, esters, ethers, lactones, and ketones.[53] This reinforces a negative zeta potential commonly found in the commercial nanodiamond powders. Positive zeta potential (typically at pH < 7) can be attained on NDs with a certain surface content of sp^2 bonding, specifically graphene-like shells that become protonated.[59] Nanodiamond aqueous colloidal solutions containing stable single particles were reported for hydrogen-treated[60] and microbead-assisted ultrasonically de-aggregated DNDs.[61]

Compared to carbon nanotubes (CNTs) and other graphite-based nanoparticles, NDs have a greater capacity to affix different functional groups to their surfaces, including modification with biologically active moieties.[62] Covalent functionalization can proceed via the different functional groups that already exist on the surface of commercial NDs, but carboxylated NDs prepared by ozone and air purification methods are popular

© 2025 The Author(s). Advanced Materials Technologies published by Wiley-VCH GmbH

2365709x, 2025, 22, Downloaded from https://advanced.onlinelibrary.wiley.com/doi/10.1002/admt.202501111, Wiley Online Library on [19/11/2025]. See the Terms and Conditions (https://onlinelibrary.wiley.com/terms-and-conditions) on Wiley Online Library for rules of use; OA articles are governed by the applicable Creative Commons License

starting materials. On the other hand, hydrogenated NDs are produced using plasma or thermal treatment at elevated temperatures, which results in the complete removal of oxygen from the surface. Other surface modifications are obtained by using wet chemistry involving the conversion of the many functional groups known in organic chemistry (e.g., photochemical chlorination, esterification, silanization), while diazonium chemistry and Diels–Alder reactions are carried out for the functionalization of graphitized NDs.

To date, NDs have found wide application in industrial, commercial, and academic settings. In particular, they have become a key platform for numerous nanoscience and nanotechnology developments.[31] The spin properties of color centers in NDs can be optically detected, which has triggered the development of high-resolution magnetometers and quantum sensors. NDs are frequently reported in biosensing and tissue engineering studies, and ND-mediated drug delivery has also been widely explored in recent years. NDs are valuable lubricant additives, while both micro- and nanosized diamond powders are used as a polishing agent due to their high wear resistance and hardness. Their embedding in metallic, ceramic, and polymeric matrices to produce mechanically reinforced composite materials for various tribological applications has become an active domain of research. Also, the recent developments related to diamond-polymer composites for thermal applications are noteworthy. In general, pristine diamond powders as well as functionalized ones are used to form diamond composites with advanced material properties, and also their processing in combination with additives in resin systems has been reported for particular applications.

3. Printing Techniques

This section provides an overview of the printing techniques utilized for materials containing diamond nano- or microparticles, which were employed to fabricate the range of system components and devices discussed in detail in Section 4. It outlines the basic principles, advantages, and limitations of these techniques to provide the necessary background for understanding their applications. Rather than an exhaustive discussion of each printing method, this chapter aims to offer a concise introduction to its key aspects, ensuring clarity and context for the subsequent sections. A comparative overview summarizing typical resolution, cost-effectiveness, scalability, main limitations, and key advantages of the discussed techniques is provided in Table S1 of the Supporting Information to complement the text.

3.1. Screen Printing

Screen printing is a widely adopted technique for fabricating structured patterns on a broad range of substrates. Its key strengths lie in the versatility, high repeatability, and compatibility with diverse materials, making it a cost-effective and scalable method for large-scale manufacturing. Screen printing is particularly suitable for flexible, stretchable, and low-cost substrates.[63] However, one limitation of this technique is its relatively low resolution compared to high-precision methods like inkjet printing (see Subsection 3.3), which may restrict its use in applications requiring fine patterning.

The screen-printing process, illustrated in **Figure 3A**, consists of three main components:[63,64] i) substrate – the surface onto which the ink is deposited; ii) screen mesh (template) – a stencil that defines the printed pattern; and iii) squeegee – a flat, rigid blade that forces the ink through the open areas of the mesh onto the substrate. The ink is transferred selectively, forming well-defined patterns. One of the major advantages of screen printing is its compatibility with various functional inks, allowing the deposition of a broad range of conductive, semiconducting, and insulating materials.[63,64] Additionally, multi-layered structures can be created through overprinting, where different materials are sequentially deposited onto the same substrate.[65,66]

The quality and performance of screen-printed structures are influenced by several critical parameters.[63–65] The composition of the ink, particularly the balance of solvents, binders, and functional particles, is essential for achieving uniform, stable deposition. Print uniformity and adhesion can be further improved through substrate pre-treatments such as plasma activation or surface modification. Screen printing offers high reproducibility due to the absence of satellite droplets and the minimization of coffee ring effects, issues more common in droplet-based techniques like inkjet printing (see Subsection 3.3). Consistent squeegee force and alignment are also crucial for ensuring uniform layer thickness across the printed area. Finally, post-processing steps such as thermal curing, UV treatment, or chemical annealing enhance the mechanical strength, conductivity, and durability of the printed structures.

Screen printing has been successfully employed in the fabrication of various diamond-based materials. This includes the use of BDD microparticle pastes for electrochemical sensors,[16,17,67–70] BDD nanosheet-enriched carbon inks for biosensing applications,[71] and NDs-containing inks for devices such as electron emission cathodes.[72]

3.2. Microcontact Printing

Microcontact printing (μCP) is a versatile and cost-effective surface patterning technique that enables the transfer of micro- and nanoscale features onto a substrate using an elastomeric stamp.[73,74] Its ability to produce high-resolution patterns without the need for complex lithographic processes has made it particularly valuable for applications in microelectronics, biosensors, and advanced materials science.[73,74]

The fundamental principle of μCP is the selective transfer of an "inked" material from a patterned polymeric stamp to a substrate.[73,74] The process includes several key steps, shown in Figure 3B. First, an elastomeric stamp, typically made from polydimethylsiloxane (PDMS), is fabricated by curing a prepolymer over a master template. This stamp, which contains a raised relief pattern, is then inked with the desired material, selectively absorbing the ink onto the raised features. When the inked stamp is brought into contact with the substrate, the ink is transferred, forming a well-defined pattern. Finally, the stamp is removed, leaving behind a structured deposition of the material. The resolution of μCP can reach sub-100 nm levels, depending on factors such as stamp quality, ink formulation, and substrate properties.

The effectiveness of μCP relies on the interaction between the stamp, ink, and substrate.[74,75] PDMS is the most commonly

© 2025 The Author(s). Advanced Materials Technologies published by Wiley-VCH GmbH

2365709x, 2025, 22, Downloaded from https://advanced.onlinelibrary.wiley.com/doi/10.1002/admt.202501111, Wiley Online Library on [19/11/2025]. See the Terms and Conditions (https://onlinelibrary.wiley.com/terms-and-conditions) on Wiley Online Library for rules of use; OA articles are governed by the applicable Creative Commons License

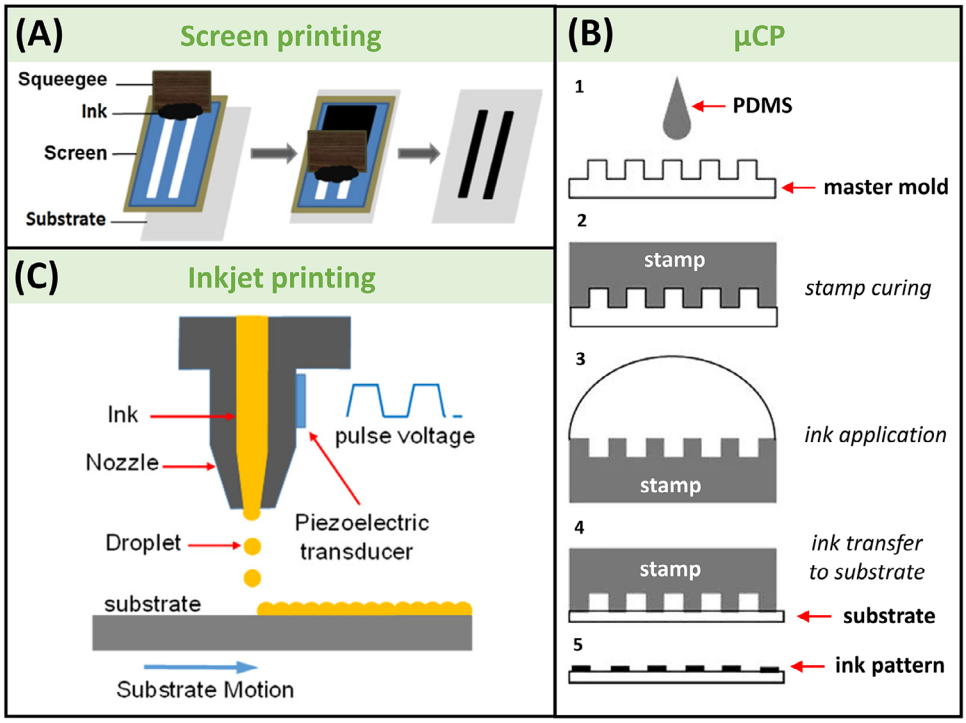


Figure 3. A) Schematic illustration of the screen-printing process, showing the deposition of ink through a patterned screen (mesh) onto a substrate using a squeegee. Reproduced with permission from ref. [91]. Copyright 2017, Elsevier. B) Step-by-step schematic of the μCP process: 1) PDMS is poured over a master pattern; 2) cured to form a flexible stamp; 3) ink is applied to the stamp; 4) the stamp is brought into contact with the substrate for ink transfer; and 5) removed, leaving behind a patterned layer. Reproduced with permission from ref. [92]. Copyright 2005, Springer. C) Working principle of piezoelectric inkjet printing, where mechanical deformation of a piezoelectric element ejects ink droplets through a nozzle with high precision. Reproduced with permission from ref. [93]. Copyright 2015, Science X.

used stamp material due to its flexibility, chemical inertness, and ease of fabrication. However, its hydrophobic nature can limit the transfer efficiency of certain polar inks, necessitating surface treatments or the use of alternative elastomers. The ink composition plays a critical role in achieving uniform and well-defined patterns, as it must selectively adhere to the substrate while minimizing unwanted spreading or diffusion. Similarly, the substrate often requires pre-treatment, such as plasma activation or chemical functionalization, to enhance adhesion and improve pattern resolution.

The technique is highly adaptable for various applications due to its compatibility with a wide range of materials and substrates, while its non-destructive nature enables the processing of delicate or flexible materials without causing damage.[75] However, μCP also faces several challenges. Ink diffusion beyond the printed areas can lead to reduced pattern reliability, particularly when working with low-viscosity inks.[75] The soft and flexible nature of PDMS stamps can also result in pattern distortion due to swelling, mechanical deformation, or buckling.[73,74] Furthermore, scaling μCP for large-area patterning remains difficult, as maintaining uniform pressure and contact over extended surfaces poses a challenge.

In the context of diamond-based fabrication, μCP has proven effective for generating patterned seeding layers using ND particles, which act as nucleation sites for subsequent CVD growth of diamond films. This method enables the scalable production of high-resolution diamond structures, including miniaturized features, supporting applications in microelectronics,[76] microelectromechanical systems (MEMS),[77] and neural research, such as promoting ordered neural cell adhesion.[78]

3.3. Inkjet Printing

Inkjet printing is a versatile, digitally controlled additive manufacturing technology that enables the precise deposition of functional materials, predominantly using a drop-on-demand mechanism.[79] This technique offers high precision, minimal material waste, and flexible patterning, making it an efficient and contactless method for printing on a wide range of substrates.[66,80]

Inkjet printing belongs to "direct-write" technologies and operates by precisely depositing ink droplets (volumes of a few pL) onto a substrate through micron-scale nozzles.[80] Unlike screen printing (described in Subsection 3.1), which relies on a stencil, inkjet printing is a digital, mask-free technique, enabling fully customizable patterns for rapid prototyping and flexible manufacturing.[66] The movement of the nozzles is software-controlled, ensuring accurate droplet placement and allowing for the fabrication of fine, high-resolution structures.

Inkjet printing techniques are categorized based on their droplet generation mechanism,[66,79] with piezoelectric inkjet printing being applied for printing nanodiamond-containing

© 2025 The Author(s). Advanced Materials Technologies published by Wiley-VCH GmbH

2365709x, 2025, 22, Downloaded from https://advanced.onlinelibrary.wiley.com/doi/10.1002/admt.202501111, Wiley Online Library on [19/11/2025]. See the Terms and Conditions (https://onlinelibrary.wiley.com/terms-and-conditions) on Wiley Online Library for rules of use; OA articles are governed by the applicable Creative Commons License

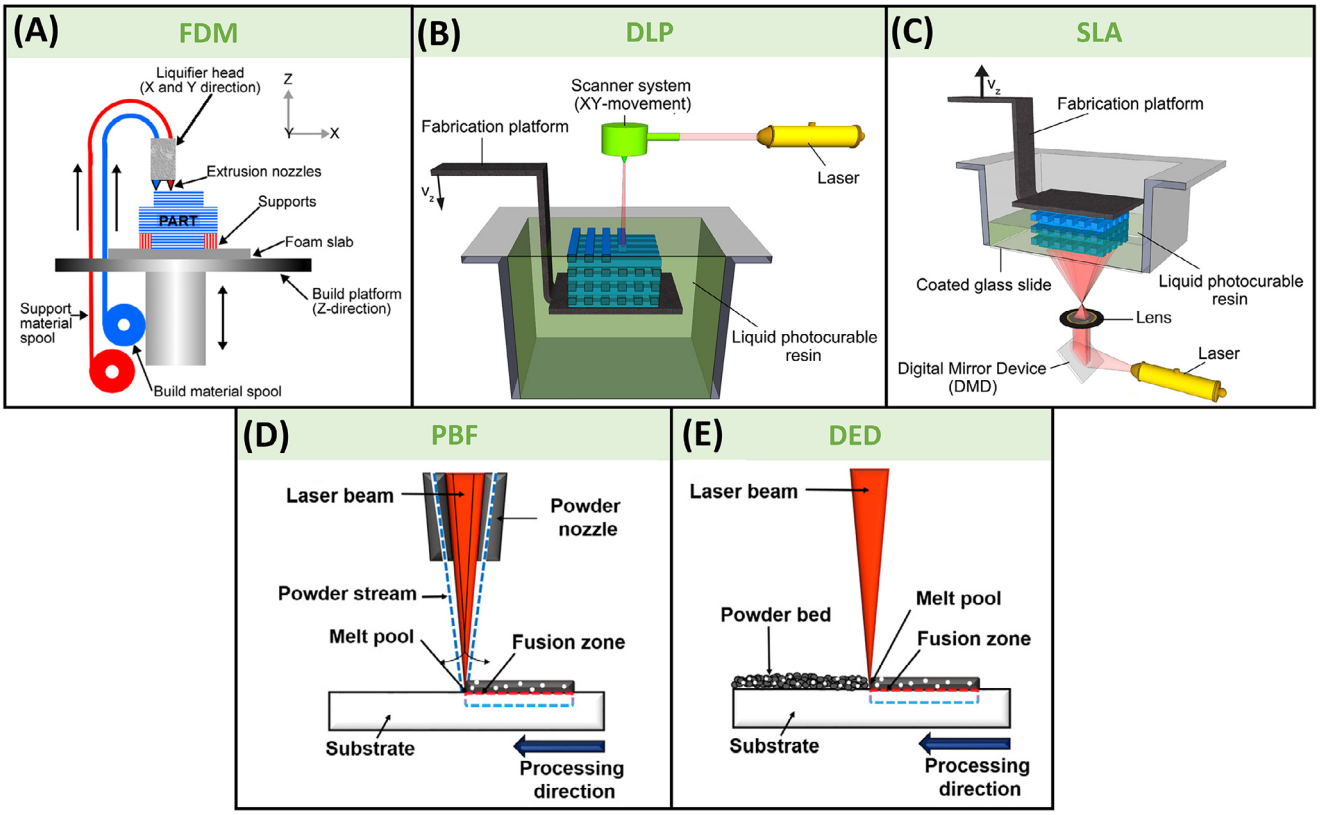


Figure 4. Schematic illustration of the working principles of representative 3D printing techniques: A) FDM – a thermoplastic filament is extruded through a heated nozzle and deposited layer-by-layer onto a build platform (Reproduced with permission from ref. [112]. Copyright 2014, MDPI.); B) DLP – a digital light projector cures entire layers of liquid photopolymer resin simultaneously to form solid structures; C) SLA – a UV laser scans and selectively cures liquid photopolymer resin layer by layer with high precision (Reproduced with permission from ref. [113]. Copyright 2012, MDPI.); D) PBF – a high-energy laser or electron beam selectively fuses regions of a powder bed to create solid parts layer by layer; and E) DED – metal wire is fed through a nozzle and melted by an electron beam as it is deposited onto a substrate (Reproduced with permission from ref. [114]. Copyright 2020, Elsevier.).

inks.[81,82] This is one of the most widely used methods, where a piezoelectric crystal deforms under an applied voltage, mechanically ejecting ink droplets from the nozzle,[79,80] as schematically illustrated in Figure 3C. This technique enables precise control over droplet size and positioning, making it ideal for high-resolution printing (down to 20–50 µm). However, it is limited by relatively low printing speeds compared to other inkjet technologies.

Ink properties such as viscosity, surface tension, and volatility must be carefully optimized to ensure stable droplet formation and deposition.[79,83] Poorly formulated inks can lead to nozzle clogging, inconsistent droplet ejection, or uncontrolled spreading on the substrate. Another major challenge in inkjet printing is the formation of satellite droplets, which can distort printed patterns and reduce resolution. The coffee ring effect, caused by uneven evaporation of solvent within the droplets, can also result in non-uniform printed features.

Similar to µCP, inkjet printing is also employed for the selective area seeding of NDs, followed by CVD growth of diamond films. However, its applications are broader, as inkjet printing has been used not only for the fabrication of patterned and miniaturized diamond structures[81,84,85] but also for mass,[82] gas,[86,87] and electrochemical sensors,[88] UV photodetectors,[89] and for controlled placement (or embedding) of NDs for quantum applications.[90]

3.4. 3D Printing Techniques

3D printing enables the layer-by-layer fabrication of complex structures with high precision, design flexibility, and minimal material waste.[94,95] The techniques used in 3D printing are broadly categorized based on the energy source and material deposition strategy into non-laser-based and laser-based methods. Non-laser-based techniques include fused deposition modelling (FDM), fused deposition modelling and sintering (FDMS), and digital light processing (DLP), while laser-based techniques encompass stereolithography (SLA) and two prominent families: powder bed fusion (PBF) and directed energy deposition (DED).[94,95] Each of these methods offers unique advantages in terms of resolution, material compatibility, scalability, and mechanical performance.

FDM, schematically depicted in **Figure** 4A, is one of the most accessible and widely adopted methods, particularly suitable for polymers and composites. It functions by extruding a thermoplastic filament through a heated nozzle, depositing the

© 2025 The Author(s). Advanced Materials Technologies published by Wiley-VCH GmbH

2365709x, 2025, 22, Downloaded from https://advanced.onlinelibrary.wiley.com/doi/10.1002/admt.202501111, Wiley Online Library on [19/11/2025]. See the Terms and Conditions (https://onlinelibrary.wiley.com/terms-and-conditions) on Wiley Online Library for rules of use; OA articles are governed by the applicable Creative Commons License

material layer-by-layer onto a build platform.[95,96] This approach is favored for its low cost and ease of use, although its resolution is limited and printed parts may exhibit visible layer lines and reduced mechanical strength. Additionally, support structures are often required for printing, adding complexity to post-processing. FDMS builds on this concept, embedding metal or ceramic powders into a thermoplastic matrix to create printable filaments.[97] After printing, the composite part undergoes debinding and sintering to produce dense, mechanically robust components. While FDMS allows affordable desktop fabrication of metal and ceramic parts, post-processing can be complex and must be precisely managed to avoid shrinkage or deformation.[97]

When working with diamond microparticles, additional considerations arise due to the material's extreme hardness and abrasiveness, which can pose challenges to standard 3D printing equipment. For instance, in FDM-based methods, diamond particles can cause accelerated wear of key printer components, such as nozzles and feeding gears. To ensure reliable and long-term operation, hardware modifications are often necessary, commonly involving the replacement of standard steel components with reinforced materials like titanium or hardened steel.[18,98] Additionally, to prevent clogging during extrusion, larger nozzle diameters (e.g., 0.8 mm) are often employed, ensuring a smooth and continuous printing process despite the presence of hard fillers.[18,98]

DLP, shown in Figure 4B, represents a digital photopolymerization technique in which entire resin layers are simultaneously cured using a digital light projector, significantly reducing the build time.[94,99] DLP offers excellent resolution and is commonly used for producing detailed parts in fields like dentistry, jewelry, and electronics. However, it is limited to photosensitive resins, which may require additional curing and typically exhibit brittle mechanical behavior.

In contrast to DLP, SLA uses a focused UV laser to selectively cure resin in a layer-by-layer scanning process (Figure 4C).[95,100] This laser-based approach achieves high accuracy and surface finish, but curing is slower than DLP, and the materials used share similar brittleness limitations, making them less suitable for high-impact applications unless reinforced with post-processing treatments or composite resins.

Among laser-based 3D printing techniques, two major families are widely used for processing polymers, ceramics, and metals: powder bed fusion (PBF) and directed energy deposition (DED).[95] In PBF, a thin layer of powder material[101,102] – polymeric, ceramic, or metallic – is spread over a build platform, and a high-energy laser selectively fuses the powder particles according to a digital design, as schematically displayed in Figure 4D. The process repeats layer-by-layer until the entire object is formed. PBF enables the fabrication of complex, high-resolution parts with excellent mechanical properties, especially when working with metals. An important advantage is that unsintered powder acts as a support during printing, eliminating the need for additional support structures.[94] However, PBF requires fine powders, controlled environments, and often post-processing to reduce porosity and improve surface finish.

DED, on the other hand, involves the focused application of energy, typically via a laser or electron beam, onto a substrate while simultaneously feeding metal powder or wire into the melt pool,[103] which is illustrated in Figure 4E. This method is particularly well-suited for repairing existing components, adding localized features, or fabricating large-scale metal parts. DED allows for precise control over material placement and composition, but generally has lower resolution compared to PBF and requires more careful thermal management to prevent defects and warping.

3D printing methods, primarily combined with diamond microparticles, have been employed in a wide range of applications, including electrochemical[18] and humidity[98] sensors, heat sinks and cooling coils for thermal management,[104–106] as well as diamond-impregnated tools such as grinding heads and wheels to enhance mechanical performance.[107–111] These applications are further discussed in Section 4.

4. Applications

Given the aforementioned broad variety in particle sizes, shapes, surface states, and targeted applications of diamond powders (see Section 2), the printing thereof, either through ink, filament, resin or powder mixture with or without solvent, surfactant, and/or modifier, typically requires a highly tailored approach and a single standard processing method does not exist. Therefore, in the following sections, the specific diamond powder characteristics and their processing prior to or during the printing, if known, will be specified per case. A comprehensive summary of the literature on diamond printing, including diamond powder type, printing technique, matrix material, and application, is available in Table S2 of the Supporting Information.

4.1. Fabrication of Patterned and Miniaturized Diamond Structures

The ability to fabricate patterned and miniaturized diamond structures has gained significant interest in various fields such as microelectronics, photonics, and sensor technologies. Diamond, owing to its exceptional mechanical, thermal, and electrical properties (see Subsection 2.1), is an ideal material for high-performance applications. However, the challenge lies in the precision fabrication of diamond structures on a microscale. The emergence of printing technologies, particularly inkjet printing and μCP, offers a promising approach to address this challenge by enabling selective seeding of diamond nanoparticles (<50 nm in size) and subsequent CVD growth. Therefore, this subsection reviews the advancements in using printing technologies to create micropatterned and miniaturized diamond structures by optimizing key factors such as ink composition, substrate surface treatment, and printing parameters, while highlighting the associated methodologies, challenges, and potential applications.

4.1.1. Droplet-Based Patterning of Diamond Nanoparticles

The initial successful efforts in using inkjet printing to pattern diamond nanogrit were made by Fox et al. almost 25 years ago.[84] In their study, commercially available diamond suspensions were mixed with water-based ink to create a printable solution, allowing for the direct deposition of diamond nanoparticles onto substrates such as glass, silicon, copper, and fused quartz. To ensure

© 2025 The Author(s). Advanced Materials Technologies published by Wiley-VCH GmbH

2365709x, 2025, 22, Downloaded from https://advanced.onlinelibrary.wiley.com/doi/10.1002/admt.202501111, Wiley Online Library on [19/11/2025]. See the Terms and Conditions (https://onlinelibrary.wiley.com/terms-and-conditions) on Wiley Online Library for rules of use; OA articles are governed by the applicable Creative Commons License

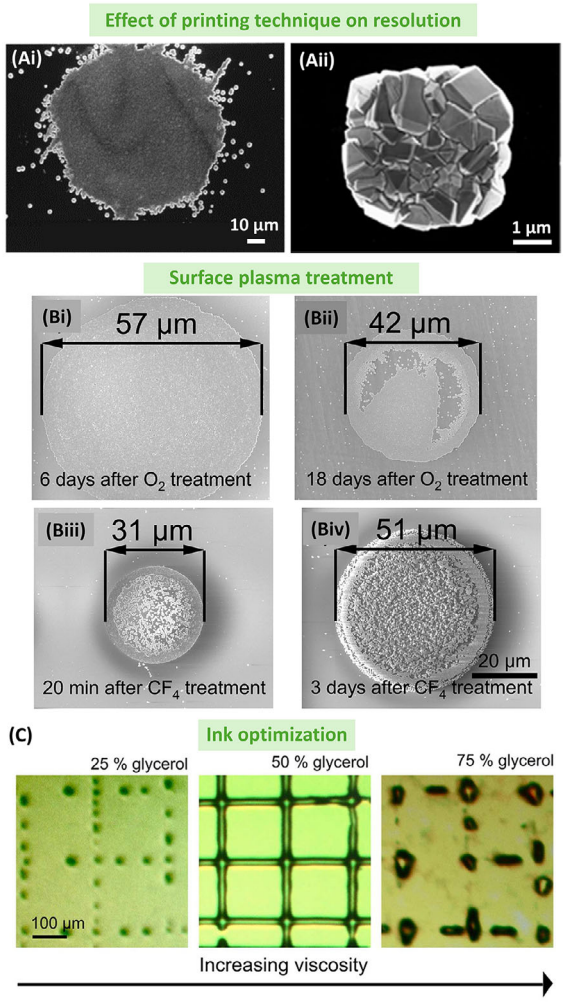


Figure 5. A) Scanning electron microscopy (SEM) images showing diamond micropatterns formed via different printing techniques: Ai) diamond dot (≈80 µm in diameter) grown by CVD for 22 h on a copper substrate, with visible splashing effects; nucleation was achieved via inkjet printing (Reproduced with permission from ref. [84]. Copyright 2000, AIP Publishing); Aii) square diamond pattern (≈4.5 µm) obtained after 4 h of CVD on a silicon substrate, with nucleation achieved by µCP (Reproduced with permission from ref. [76]. Copyright 2011, American Chemical Society). B) Evolution of the diameter of multiple inkjet-printed ND-containing dried-up droplet patterns as a function of the time after (top) O_2 plasma and (bottom) CF_4 plasma pre-treatment. Resulting droplet patterns after Bi) 6 and Bii) 18 days for O_2 plasma, and Biii) 20 min and Biv) 3 days for CF_4 plasma. Reproduced with permission from ref. [116]. Copyright 2024, American Chemical Society. C) Optical microscope images of grids printed using ND-containing inks on a glass substrate, applying a micropipette. The three images differ in glycerol percentage, which increases from left to right. Optimum printing is observed using an ink containing 50 wt.% glycerol (middle image). Reproduced with permission from ref. [117]. Copyright 2015, American Chemical Society.

uniform wettability, glass and silicon substrates were treated with a surfactant. The resolution of the printed patterns was decent, achieving dot-shaped features as small as 80 µm, as depicted in **Figure** 5Ai. However, the low density of printed ND seeds required prolonged diamond CVD processes, extending over 20 h to form large-grained polycrystalline diamond films, often with scattered diamond particles surrounding the patterns due to ink splashing (Figure 5Ai).

Subsequent studies, further expanding on Fox's pioneering work,[84] addressed the splashing effects during inkjet printing, along with challenges related to ink viscosity and jetting resistance.[81,85] In these works, ink composition was optimized by mixing ND powder with ethylene glycol,[81,85] which then resulted in inkjet-printed lines as narrow as 40 µm on silicon and quartz substrates.[85] Approximately 3 h long CVD process was required to form continuous polycrystalline diamond films due to higher concentration of NDs; however, one must balance between the seeding density and risk of clogging the inkjet nozzles. The CVD growth time was further reduced to only 15–20 min in,[81] achieving pinhole-free nanodiamond films of desired patterns with minimal splashing. This improvement was attributed to a carefully formulated ND suspension in ethylene glycol with optimal viscosity, which suppressed previous problems with jetting resistance and simultaneously enabled a very high surface density of ND seeds to form an almost continuous film even before the CVD process. Additionally, drop spacing was identified and optimized as a key parameter for achieving fine patterning.[81]

More recent works have explored the use of inkjet printing for seeding ND particles to create nanocrystalline diamond coatings on glass.[115,116] In,[115] the authors demonstrated the ability to deposit NDs with very efficient use of ink, achieving droplet volumes as low as 1 pL, resulting in droplet diameters of 12.4 µm. The study reported successfully printed patterns with a resolution of 87 µm. Moreover, by printing three layers with a 5 µm shift between each layer, the researchers averaged out inhomogeneities from nozzle trajectory and capillary flow effects, further enhancing pattern quality. Next, the effects of various surface treatments, UV-ozone, O_2 plasma, and CF_4 plasma, on the wetting properties of fused silica substrates were investigated,[116] which are crucial for enhancing the resolution of inkjet-printed patterns (Figure 5B). It was found that UV-ozone and O_2 plasma treatments produced hydrophilic surfaces, whereas CF_4 plasma treatment resulted in hydrophobic surfaces, which significantly improved printing resolution. Specifically, CF_4 plasma treatment enabled the generation of high-resolution patterns with printed droplet sizes as small as 30 µm in diameter (see Figure 5Biii). The study also demonstrated that the timing between surface treatment and printing was critical: samples printed within 2 h of CF_4 plasma treatment maintained a contact angle sufficient to regulate droplet size, starting at 31 ± 1 µm after 20 min. However, this hydrophobicity was lost within a day due to the decay of the fluorocarbon layer created by the CF_4 treatment (see Figure 5Biv). Moreover, the study highlighted a trade-off between achieving high-resolution patterns and ensuring homogeneous surface coverage. While hydrophobic surfaces facilitated high-resolution printing, achieving uniform coverage required more hydrophilic surfaces to reduce capillary-driven flow behavior. The researchers suggested optimizing the timing between surface modifications and printing to balance these factors, ensuring both high resolution and homogeneity.

© 2025 The Author(s). Advanced Materials Technologies published by Wiley-VCH GmbH

2365709x, 2025, 22, Downloaded from https://advanced.onlinelibrary.wiley.com/doi/10.1002/admt.202501111, Wiley Online Library on [19/11/2025]. See the Terms and Conditions (https://onlinelibrary.wiley.com/terms-and-conditions) on Wiley Online Library for rules of use; OA articles are governed by the applicable Creative Commons License

4.1.2. Stamp-Assisted and Direct Micropatterning

Unlike inkjet printing, which is limited by its resolution to feature sizes of typically several dozen microns, μCP offers high resolution dependent on a PDMS stamp, potentially reaching below 100 nm.[76] The process uses DNDs as small as 5 nm to achieve high nucleation densities (≈10^{11} cm^{-2}), which are crucial for synthesizing continuous, pinhole-free diamond films in a short time. Enhanced adhesion and uniformity of the diamond patterns are achieved by using an oxidized PDMS stamp and a poly(methylmethacrylate) (PMMA) layer on the silicon substrate. The μCP technique has demonstrated the ability to produce well-defined diamond patterns, including 50 μm square structures with uniform edges and sharp corners after just 2 h of layer growth. Even finer patterns have been achieved, such as 2.5 μm squares, which exhibited only a 3.6% expansion after 1.5 h of diamond deposition. However, with extended deposition times, the final pattern size increased significantly; for example, after 4 h of deposition, the pattern size grew from 2.5 to 4.5 μm (see Figure 5Aii). Despite this expansion, the overall shape of the patterns remained unchanged. Additionally, high-quality microcrystalline diamond circles with diameters as small as 8 μm were fabricated through prolonged deposition from an initial 4 μm printed circle.[76]

In a recent study, μCP was demonstrated as a simple yet effective method for the bottom-up fabrication of diamond MEMS cantilevers.[77] The process began with the preparation of an optimized ND-containing ink composed of thermally refined DNDs (≈70 nm) dispersed in an acetone solution with fine-tuned pH (8.5), ionic concentration (0.01 mol L^{-1}), and PMMA content to ensure colloidal stability. A PDMS stamp, replicated from a silicon master mold with patterned cantilever arrays (100 μm wide, 500–2000 μm long, 2 μm deep), was cleaned and oxygen plasma-treated prior to inking via spin-coating. The ND-containing pattern was transfer-printed onto a preheated silicon (100) substrate, followed by CVD to grow the diamond layer. The final cantilever structures were released using wet chemical etching in a KOH-isopropanol bath, avoiding lattice damage associated with dry etching. This approach produced relatively high-density ND seeding layers (≈10^{9} cm^{-2}; NDs clusters had an average size of ≈100 nm), crucial for selective diamond growth, and enabled the fabrication of high-quality, suspended diamond MEMS structures. These results demonstrate that combining the μCP method with ND seeding enables precise and scalable patterning as well as its potential as a cost-effective strategy for producing diamond-based microdevices suitable for sensing and quantum technologies.

Lastly, a "direct-write" printing technique was developed using a computer-controlled micropipette.[117] This method allowed for the deposition of nanodiamond tracks with picolitre volumes of liquid, achieving line widths as narrow as 2 μm. This was accomplished by optimizing ink composition, particularly focusing on the effects of glycerol content. Different concentrations of glycerol were tested (demonstrated in Figure 5C), with the optimum viscosity for printing found in a mixture of 50 wt.% glycerol and 50 vol.% deionized water. This formulation significantly improved print quality by reducing the "coffee-ring" effect, which occurs when the ink dries unevenly, leading to a higher concentration of NDs at the edges of the pattern. The glycerol also slowed the evaporation rate of water, ensuring a more uniform deposition of NDs across the substrate. Before seeding, substrates such as silicon, SiO_2, and quartz were meticulously cleaned and treated with UV-ozone to improve surface wettability. The resulting nanodiamond patterns were then grown into nanocrystalline diamond films over periods ranging from 30 min to 4 h, depending on the desired thickness and uniformity.

4.2. Sensors

Using various printing techniques, researchers have developed diamond-particle-based printed sensors that serve a wide range of applications, from mass and gas detection to electrochemical sensing. These printed sensors offer significant advantages in terms of fabrication flexibility, cost-effectiveness, and scalability, enabling rapid prototyping and customization for specific sensing tasks. This chapter reviews recent progress in diamond-based printed sensors, emphasizing how these technologies improve sensitivity, precision, and adaptability across various analytical applications.

4.2.1. Mass and Gas Sensors

In 2019, Sartori et al.[82] introduced a low-cost, lithography-free method for fabricating diamond-based micro-resonators using inkjet printing. In this process, a standard desktop inkjet printer was used to deposit water-based nanodiamond ink onto a substrate, creating spots ≈50–60 μm in diameter. These spots were then grown into nanocrystalline diamond films of ≈1 μm thickness through CVD and suspended using reactive ion etching; the fabrication is schematically depicted in **Figure 6A**. Laser interferometry analysis revealed that the fabricated resonators exhibited resonance frequencies between 9 and 30 MHz, with high quality (Q) factors exceeding 10^4, and a figure of merit ($f_n \times Q$) reaching ≈2.5×10^{11} Hz in vacuum. When applied as mass sensors, the inkjet-printed diamond resonators demonstrated exceptional sensitivity. After gold deposition, the resonators achieved mass responsivities up to 981 Hz fg^{-1} and ultra-high mass resolution, with values reaching 278 ± 48 zg, which surpasses many traditional lithography-based sensors. This work demonstrates the potential of direct inkjet printing for creating high-performance, low-cost diamond-based mass sensors.

Inkjet printing was also utilized for fabricating gas sensors.[86,87] Particularly, a quartz crystal microbalance (QCM) gas sensor with an inkjet-printed ND (1–5 nm) sensitive layer was developed for detecting low concentrations of gases such as ammonia and acetone, as well as different humidity levels.[86] The nanocrystalline morphology of the diamond layer provided a large surface area for gas adsorption, significantly enhancing sensitivity, particularly to ammonia. The sensor exhibited a frequency shift of 38 Hz in response to ammonia, three times higher than a QCM sensor coated with ZnO. Building on this approach, the gas-sensing capabilities of inkjet-seeded, CVD-grown hydrogenated nanocrystalline diamond (NCD) layers were explored under UV-LED illumination by the same group.[87] The sensor was fabricated by selectively depositing DND ink onto interdigital electrodes, followed by CVD growth of

© 2025 The Author(s). Advanced Materials Technologies published by Wiley-VCH GmbH

2365709x, 2025, 22, Downloaded from https://advanced.onlinelibrary.wiley.com/doi/10.1002/admt.202501111, Wiley Online Library on [19/11/2025]. See the Terms and Conditions (https://onlinelibrary.wiley.com/terms-and-conditions) on Wiley Online Library for rules of use; OA articles are governed by the applicable Creative Commons License

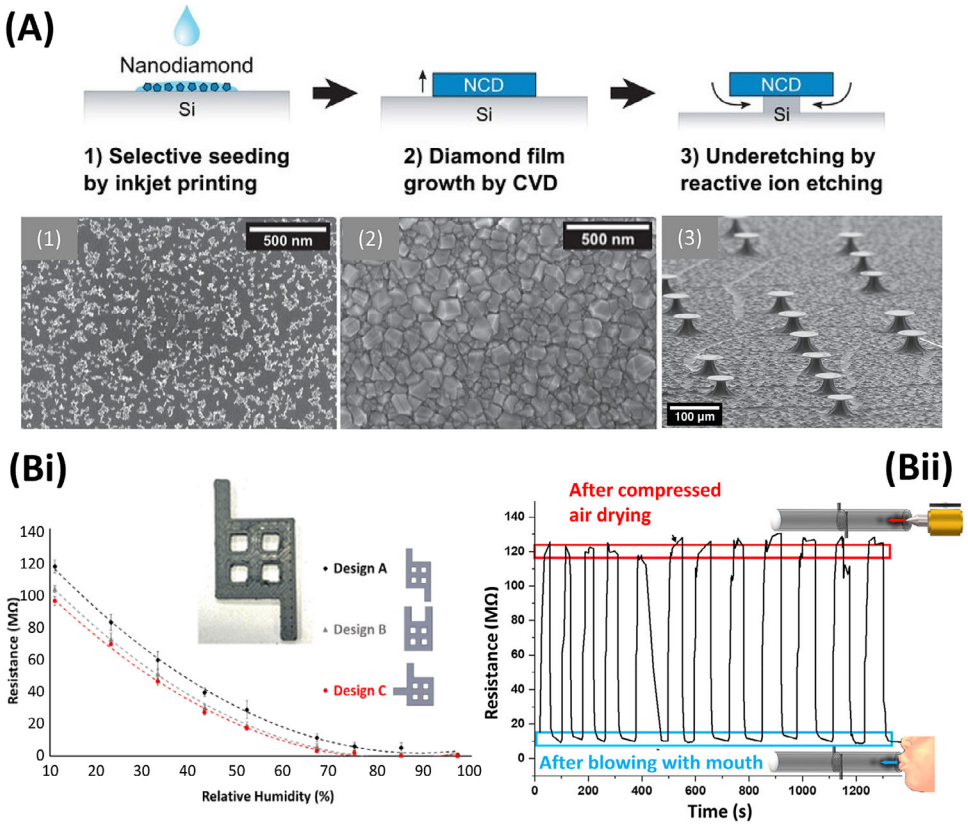


Figure 6. A) Schematic representation of the three-step fabrication process for diamond micro-disk resonators using inkjet printing, accompanied by corresponding SEM images: 1) printed droplet composed of clustered diamond nanoparticles; 2) droplet after CVD growth, forming a closed nanocrystalline diamond film; 3) final suspended diamond micro-disk resonators. Reproduced with permission from ref. [82]. Copyright 2019, Wiley. B) Performance of 3D-printed humidity sensors prepared by FDM: Bi) Comparison of three different 3D-printed electrode designs, showing sensor resistance as a function of relative humidity. Inset: Photograph of the humidity sensor based on Design A. Bii) Dynamic response of the 3D-printed humidity sensor (Design A) positioned between two plastic tubes, demonstrating sensitivity to alternating flows of compressed dry air and human breath. Reproduced with permission from ref. [98]. Copyright 2020, American Chemical Society.

a hydrogen-terminated NCD layer. The resulting NCD sensors were tested for detecting gases such as NH_3, NO_2, and O_2 at ppm levels, with the sensor's response measured as a relative change in resistance.

In addition, a 3D-printable composite material for humidity sensing was developed, consisting of BDD microparticles (60 wt.%) and lithium chloride (LiCl) (2 wt.%) within an acrylonitrile butadiene styrene (ABS) matrix, and fabricated using a FDM 3D printer.[98] In this configuration, the BDD microparticles formed electrically conducting paths, while LiCl acted as the humidity-sensitive component. Scanning electron microscopy confirmed the uniform distribution of BDD and a thin LiCl layer throughout the matrix, forming a network that enabled humidity detection. The sensor exhibited a 125-fold resistance change across relative humidity levels from 11% to 97% (shown in Figure 6Bi), demonstrating high sensitivity. When tested with human breath cycles, the sensor provided rapid response and recovery times of 13 and 60 s, respectively, making it suitable for real-time humidity monitoring (Figure 6Bii). Besides, the 3D-printing capability of this composite material allowed for customized sensor designs, such as a sensor integrated within gas pipelines to detect moisture contamination in nitrogen supplies, a setup difficult to achieve with traditional multicomponent humidity sensors. This novel approach shows promise for on-demand manufacturing of humidity sensors for both environmental and industrial applications.

4.2.2. Electrochemical Sensors

Three printing techniques, namely inkjet, screen, and 3D (FDM) printing, have been used to develop electrodes and sensors based on conductive BDD. The first approach involves direct inkjet printing of nanodiamond-containing ink onto silicon-based substrates to create three-electrode sensor chips.[88] Optimized and continuous inkjet-printed features were obtained using a glycerol-based nanodiamond ink (0.4% vol wt^{-1}), silicon substrates pre-treated with oxygen plasma followed by air exposure, and a dot density of 750 drops (9 pL volume each) per inch. After drying, the micropatterned substrate underwent chemical vapor deposition to grow a uniform thin-film BDD layer, which functioned as both the working and counter electrodes (see **Figure** 7A). Commercial silver ink was then inkjet-printed to complete the sensor chip with a reference electrode. This

© 2025 The Author(s). Advanced Materials Technologies published by Wiley-VCH GmbH

2365709x, 2025, 22, Downloaded from https://advanced.onlinelibrary.wiley.com/doi/10.1002/admt.202501111, Wiley Online Library on [19/11/2025]. See the Terms and Conditions (https://onlinelibrary.wiley.com/terms-and-conditions) on Wiley Online Library for rules of use; OA articles are governed by the applicable Creative Commons License

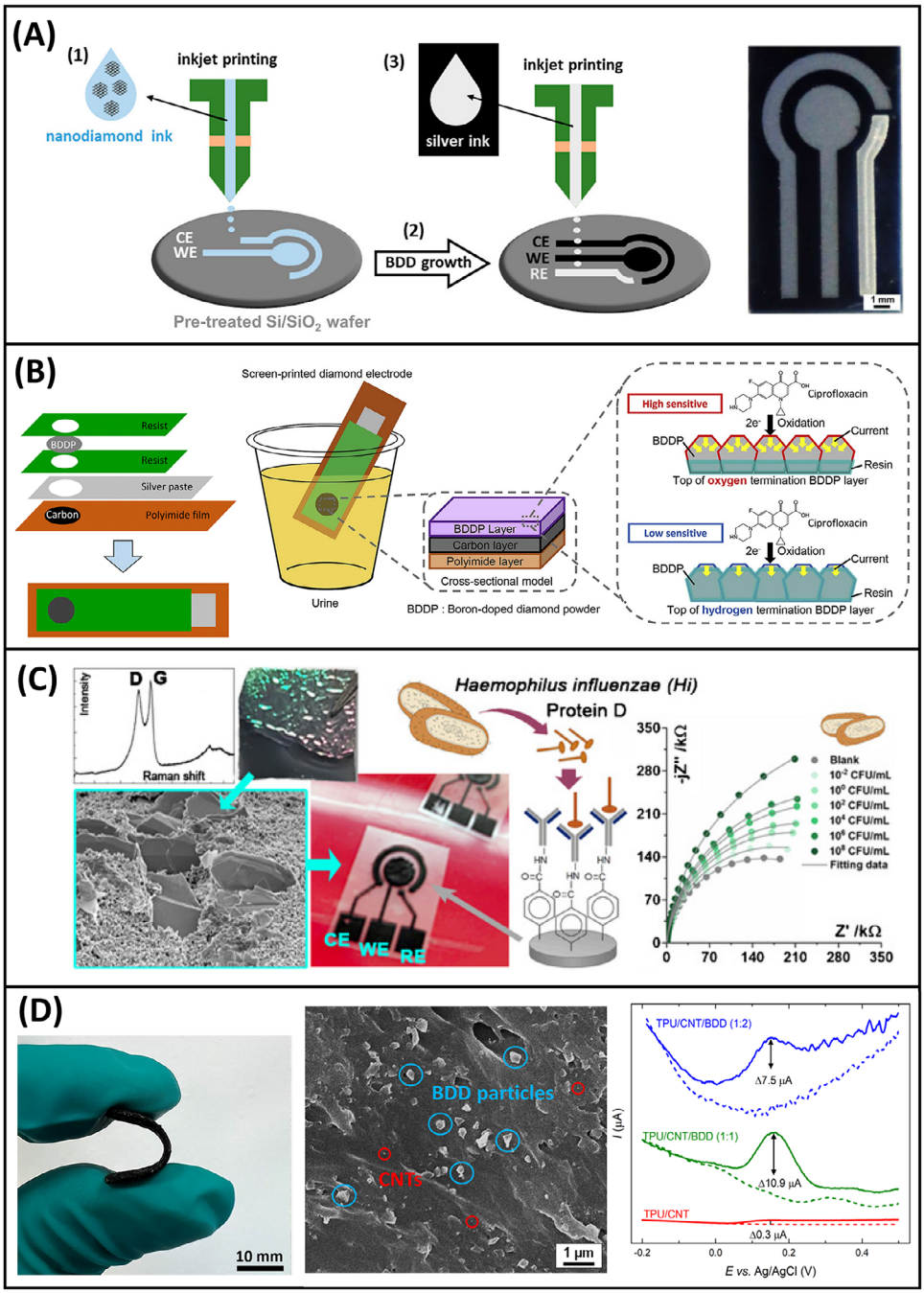


Figure 7. A) Schematic of the fabrication process for the inkjet-printed BDD three-electrode sensor chip: 1) Nanodiamond ink was inkjet-printed onto a pre-treated Si or SiO_2 wafer to define the working and counter electrodes. 2) Selectively seeded areas underwent CVD to grow a uniform BDD layer. 3) A silver reference electrode was then added via inkjet printing to complete the sensor. An optical image of the fully fabricated sensor is shown on the right (scale bar: 1 mm). Reproduced with permission from ref. [88]. Copyright 2023, American Chemical Society. B) Schematic illustration of the fabrication procedure for the BDDP-based screen-printed electrode. The electrode is applied for the detection of the antibiotic ciprofloxacin in urine samples, demonstrating enhanced sensitivity with oxygen-terminated BDDP layers. Reproduced with permission from.[17,69] Copyright 2016, American Chemical Society. Copyright 2020, Elsevier. C) Top-view SEM image (cyan frame) of the BDDP screen-printed electrode shown in the accompanying photograph. Raman spectrum of the carbon paste mixed with BDD foil is presented, along with Nyquist plots from EIS measurements at varying concentrations of *Haemophilus influenzae*, detected using the receptor-functionalized BDDP-based biosensor. Reproduced with permission from.[71] Copyright 2023, Springer. D) Optical image (left) illustrating the flexibility of the 3D-printed composite electrode. Cross-sectional SEM image (middle) shows the distribution of fillers – BDD particles and CNTs, with selected particles highlighted – within the TPU matrix. Differential pulse voltammograms of dopamine are presented (right) for three electrode compositions: TPU/CNT (red), TPU/CNT/BDD (1:1) (green), and TPU/CNT/BDD (1:2) (blue). Reproduced with permission from ref. [18] Copyright 2024, American Chemical Society.

© 2025 The Author(s). Advanced Materials Technologies published by Wiley-VCH GmbH

2365709x, 2025, 22, Downloaded from https://advanced.onlinelibrary.wiley.com/doi/10.1002/admt.202501111, Wiley Online Library on [19/11/2025]. See the Terms and Conditions (https://onlinelibrary.wiley.com/terms-and-conditions) on Wiley Online Library for rules of use; OA articles are governed by the applicable Creative Commons License

sensor demonstrated effective electrochemical detection of various organic compounds with different structural motifs, including glucose, ascorbic acid, uric acid, tyrosine, and dopamine, and its performance was successfully compared with commercially available "screen-printed" BDD electrodes. This chip-based fabrication method allows for rapid prototyping of diverse small-scale electrode designs and BDD microstructures, potentially enhancing sensor performance and enabling repeated use.

Considerable research has been conducted on screen-printed BDD electrodes.[16,17,67–71] Notably, Kondo's group developed a process in which intrinsic diamond powder was first coated with a BDD layer in a CVD reactor. The coated BDD powder (BDDP) was then mixed with polyester (PES) resin dissolved in 2-butanone and isophorone to create a BDDP paste, which was subsequently used to fabricate screen-printed BDD electrodes.[16,17,67–70] Sequential printing of silver ink as an electrical lead, carbon ink as a current collector, resist ink as a mask to prevent silver dissolution into the electrolyte solution, and BDDP ink onto a polyimide film produced a BDDP-printed electrode, as illustrated in Figure 7B. The group investigated various parameters affecting the electrochemical behavior of screen-printed BDD electrodes, including the ratio of BDD powder to polyester resin,[17] BDD particle size,[68] and surface termination (as-grown, hydrogen-terminated, and oxygen-terminated).[69,70] At high BDDP content, the printed electrodes displayed electrochemical characteristics typical of a planar electrode with a linear diffusion mode, attributed to the dense packing of BDDP on the electrode surface. In contrast, a reduction in BDDP content shifted the diffusion mode from linear to hemispherical, likely due to the formation of island-like conductive domains, ranging from several micrometers to several tens of micrometers in size, which induced microelectrode behavior. Among the printed electrodes, those with the largest BDDP particles (350–3500 nm) exhibited the widest potential window, the lowest background current, and an absence of redox peaks associated with sp^2 carbon impurities. Microscopic analysis further revealed that oxygen-terminated BDDPs were only partially covered with PES resin, while hydrogen-terminated BDDPs were fully encapsulated, a distinction that influenced the electrochemical behavior of the screen-printed electrode. These electrodes were successfully applied in sensing strategies for ascorbic acid, 8-hydroxy-2′-deoxyguanosine,[17] ciprofloxacin[69] (see Figure 7B), and L-cysteine.[70] Surface modification with cobalt phthalocyanine allowed for the detection of hydrogen peroxide, while glucose-oxidase-immobilized cobalt phthalocyanine enabled glucose detection.[67]

Another work focused on the development of BDD nanosheet volume-enriched screen-printed carbon electrodes.[71] The initially MWCVD-produced BDD foils were mechanically removed from the tantalum substrate and were then placed in the ceramic grinder for 15 min. The resulting ground BDD foil was added to a commercial carbon paste and mixed until a homogeneous mass was obtained. The ratio of diamond foil to paste was 4%. These foil fragments were strongly bonded together with carbon paste. The size of individual BDD foil flakes was ≈2 µm, whilst the conductive carbon particles within the used paste were up to 100 nm in size and stuck together to form a continuous layer with small pores. This platform was used as a biosensor, on which an anti-protein D antibody was anchored to enable the detection of Protein D produced by the bacteria *Haemophilus influenzae* (Hi) (see Figure 7C). The developed biosensor exhibited a high level of sensitivity and selectivity toward protein D and Hi. Potential applications for rapid biological and medical disposable sensors have thus been demonstrated.

Besides, some studies report on "screen-printed" BDD electrodes for detecting various compounds, though in these cases, the BDD layer is commercially produced by thin-film chemical deposition, and only the reference and counter electrodes on the sensing chip are truly screen-printed.[118–121] Similarly, laboratory-made screen-printed sensing chips, however, with chemically deposited BDD film serving as the working electrode, have been developed and applied for electrochemical detection.[122–126]

In a recent study, fused deposition modelling (FDM) was employed to fabricate flexible electrodes composed of BDD microparticles and multi-walled carbon nanotubes (CNTs) embedded in a thermoplastic polyurethane (TPU) matrix (displayed in Figure 7D). Two TPU/CNT/BDD composite filaments with different CNT:BDD ratios (1:1 and 1:2) were developed and compared to a TPU/CNT reference. Scanning electron microscopy confirmed a homogeneous distribution of the conductive fillers without aggregation. The introduction of BDD significantly enhanced the electrical performance, with the CNT:BDD–1:2 ratio composite showing a tenfold increase in conductivity (1.2 S m^{-1}) compared to the TPU/CNT. Notably, a surface activation step involving partial TPU dissolution in dimethylformamide further enhanced the electrode performance. Electrochemical characterization using redox couples ($[Ru(NH_3)_6]^{3+/2+}$ and $[Fe(CN)_6]^{3-/4-}$) revealed improved electron transfer kinetics for BDD-containing composites, reflected by reduced peak-to-peak separations and increased heterogeneous electron transfer rate constants (up to 1.1×10^{-3} cm s^{-1}). The TPU/CNT/BDD flexible electrodes also demonstrated reliable dopamine detection, showing distinct oxidation peaks, while the TPU/CNT electrode lacked a clear signal (see Figure 7D). These results highlight the synergistic benefits of combining BDD and CNTs in a printable flexible matrix and underscore the potential of FDM for developing next-generation, customizable diamond-based electrochemical devices.

To sum up, the development of printable BDD-based electrodes has enabled the rapid prototyping of robust, sensitive, and cost-effective electrochemical sensors. These printed electrodes demonstrate high performance in detecting a variety of analytes, including biomolecules and biologically active organic compounds, highlighting their potential for widespread application in environmental monitoring, healthcare, and biosensing. As printing techniques continue to evolve, BDD-based sensors are expected to become even more versatile and accessible for both research and commercial use.

4.3. Thermal Management

As modern electronic devices become increasingly compact and power-dense, effective thermal management is critical to maintaining their performance, stability, and longevity. Conventional cooling methods often fall short in meeting the demands of miniaturized, high-power systems, driving the need for advanced materials with superior heat dissipation capabilities. Diamond,

© 2025 The Author(s). Advanced Materials Technologies published by Wiley-VCH GmbH

2365709x, 2025, 22, Downloaded from https://advanced.onlinelibrary.wiley.com/doi/10.1002/admt.202501111, Wiley Online Library on [19/11/2025]. See the Terms and Conditions (https://onlinelibrary.wiley.com/terms-and-conditions) on Wiley Online Library for rules of use; OA articles are governed by the applicable Creative Commons License

renowned for its exceptional thermal conductivity (see Subsection 2.1), has emerged as a highly attractive filler in polymer composites for thermal management applications. Notably, the thermal conductivity of synthetic diamond microparticles, commonly used in these systems, has been shown to increase markedly with particle size, from ≈400 to 2000 W m^{-1} K^{-1}, as the particle diameter increases from 20 to 300 µm, approaching values comparable to bulk diamond.[127] This size-dependent behavior, linked to defect density and phonon scattering, is essential in optimizing the design of thermally conductive composites. In parallel, recent advances in 3D printing have further expanded the potential of diamond-polymer materials by enabling the fabrication of customized, efficient heat sinks and cooling components. This chapter highlights studies that exploit various 3D printing techniques to fabricate diamond-based composites for effective thermal management.

Kalsoom et al.[104] incorporated synthetic diamond (D) microparticles (2–4 µm) into an acrylate polymer (AP) matrix at loadings of 10%, 20%, 25%, and 30% (w v^{-1}), and used SLA to 3D-print heat sink structures. A significant improvement in thermal conductivity occurred at 30% (w v^{-1}), where interconnected diamond aggregates were formed (see SEM images in **Figure** 8A), and drastically enhanced heat transfer. The APD-30 composite material reduced the time required to heat a surface to 60 °C by 30% compared to lower-content composites, demonstrating a more than 200% improvement in heat transfer efficiency due to the formation of a highly interconnected diamond microparticle network. This composite material was successfully used to 3D-print prototype heat sinks (see Figure 8B) and coiled cooling systems, which exhibited exceptional thermal management capabilities. A heating system set at 100 °C was used to assess the heat transfer performance of printed heat sinks made from basic AP resin and APD composite material. Thermal imaging showed that the APD-30 composite heat sink maintained temperatures 5–8 °C higher than the AP heat sink across all measured points, indicating improved heat distribution away from the heated surface (Figure 8B). Further, in a 3D-printed coiled cooling system, the APD-30 composite reduced water temperature from 39 to 25 °C (room temperature) as it passed through the system, highlighting its potential for fluidic cooling devices and heat sinks. The study also confirmed that the inclusion of diamond microparticles did not negatively impact the thermal stability of the acrylate polymer. The composite maintained thermal stability and structural integrity, with thermogravimetric analysis showing no degradation and only slight reductions in the thermal expansion coefficient.

The same type of HPHT diamond microparticles (2–4 µm) was also integrated into an ABS polymer matrix at concentrations of 37.5 wt.% and 60 wt.%, and the resulting filament was used in a low-cost FDM printer, which was customized to handle the highly abrasive nature of diamond.[106] The incorporation of microdiamonds significantly enhanced the thermal conductivity of the composite, with ABS's thermal conductivity increasing from 0.17 to 0.94 W m^{-1} K^{-1}, a more than five-fold improvement for the 60 wt.% diamond composite. Complex heat sink structures with winged designs were 3D-printed and demonstrated a 42% improvement in heat dissipation compared to pure ABS heat sinks. Notably, the material was recyclable: waste prints were dissolved in acetone and re-extruded into functional filaments without loss of performance. This approach demonstrates a practical and sustainable route to thermally efficient, geometrically complex cooling components using desktop-scale 3D printing.

Further expanding on hybrid fillers, another study[105] employed HPHT diamond microparticles (2–4 µm) in combination with boron nitride (BN) nanoparticles (<150 nm) dispersed in a TPU matrix. Using pneumatic extrusion-based 3D printing, the authors fabricated flexible, self-supporting heat sink structures (see inset in Figure 8Ci). A 16.7 wt.% loading of each filler resulted in a nine-fold increase in tensile modulus and a 126% improvement in thermal conductivity compared to neat TPU. This thermal enhancement is attributed to the synergistic effect of the two fillers: the BN nanoparticles bridge the gaps between microdiamond particles, forming continuous heat conduction pathways. Under bottom heating at 55 °C, the composite heat sink's surface reached temperatures ≈4 °C higher than that of neat TPU, as shown in Figure 8C, confirming the improved thermal flux due to the embedded filler network. Despite the absence of surface modification, the direct inclusion of both filler types into the matrix yielded excellent dispersion and performance. The printed structures showed high resolution, uniform layer stacking, and excellent flexibility, making them suitable for stretchable and soft microelectronic applications.

Finally, Chen et al. demonstrated the use of DLP-based additive manufacturing to fabricate diamond/SiC composites with high thermal conductivity for electronic 3D-packaging applications.[128] The process involved a specially formulated photopolymerizable slurry containing micrometer-sized (ranging from 5 to 40 µm) diamond particles dispersed in a 405 nm light-curable resin, which was printed layer-by-layer using a DLP module. Following light curing, the green bodies were pyrolyzed and subjected to reactive melt infiltration with molten silicon, resulting in dense diamond/SiC composites. These composites achieved excellent thermal properties, including a thermal conductivity of 246 W m^{-1} K^{-1} and a low coefficient of thermal expansion (3.36 ppm K^{-1}), values closely matching those required for silicon chip packaging. The study also demonstrated that combining large (40 µm) and small (5–10 µm) diamond particles improved both the packing density and thermal performance. This work showcases the capability of DLP-based 3D printing to produce high-performance thermal management materials with complex geometries for advanced electronic applications.

4.4. Machining Tools

Diamond is well known for its unparalleled hardness and thermal conductivity, and high resistance to wear, and it also has the ability to form extremely sharp edges.[129] Because of these characteristics, it is the ideal abrasive material for cutting, grinding, and polishing applications in a variety of industries, including mining, construction, automotive, and electronics. The price of diamonds has decreased by two orders of magnitude as a result of the technological advances in diamond synthesis over the past few decades. Consequently, diamonds are widely used these days and dominate multiple segments of the abrasives and abrasive tools markets because of their ability to machine a wide range of materials, including metals, ceramics, and composites. Diamond tools can be divided into ceramic, metal, and resin types based

© 2025 The Author(s). Advanced Materials Technologies published by Wiley-VCH GmbH

2365709x, 2025, 22, Downloaded from https://advanced.onlinelibrary.wiley.com/doi/10.1002/admt.202501111, Wiley Online Library on [19/11/2025]. See the Terms and Conditions (https://onlinelibrary.wiley.com/terms-and-conditions) on Wiley Online Library for rules of use; OA articles are governed by the applicable Creative Commons License

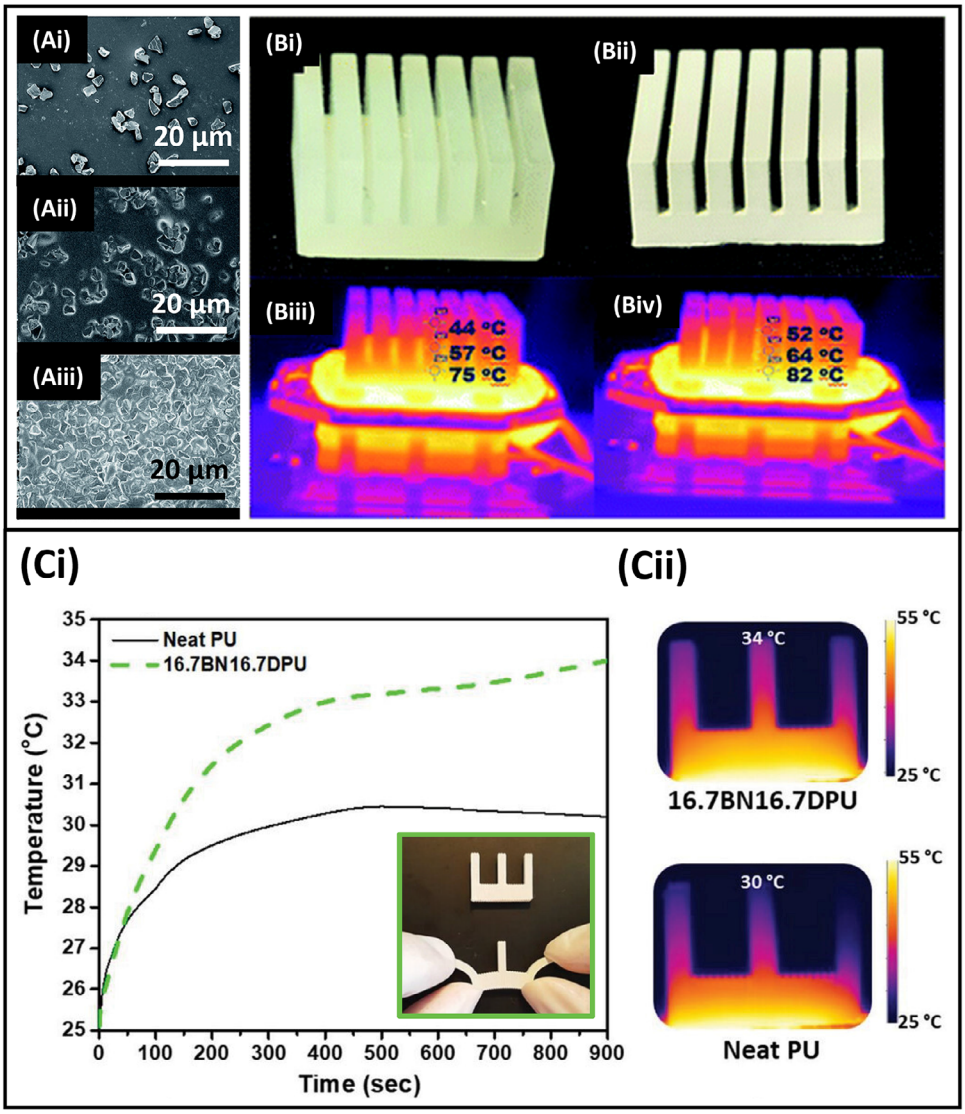


Figure 8. A) SEM cross-sectional images of composites fabricated using stereolithographic 3D printer with synthetic diamond microparticles (2–4 µm) dispersed in an acrylate polymer matrix at Ai) 10% (w v^{-1}), Aii) 25% (w v^{-1}), and Aiii) 30% (w v^{-1}) loadings. B) Comparison of 3D-printed heat sink performance: Bi) heat sink made from commercial acrylate resin, Bii) heat sink printed using 30% (w v^{-1}) diamond composite, Biii) IR image of the polymer heat sink after 10 min of heating at 100 °C, and Biv) IR image of the composite heat sink under the same conditions. Reproduced with permission from ref. [104]. Copyright 2016, Royal Society of Chemistry. C) Thermal evaluation of heat sinks fabricated via pneumatic extrusion-based 3D printing: Ci) Temperature–time curves measured at the top of the middle fin for neat thermoplastic polyurethane (PU) and the 16.7BN–16.7D–PU composite. Inset: Photograph of the flexible 3D-printed 16.7BN–16.7D–PU heat sink, demonstrating its bendability. Cii) IR images captured after 15 min of heating the base of the objects at 55 °C, illustrating the temperature distribution in both materials. Reproduced with permission from ref. [105]. Copyright 2023, Wiley.

on their matrix material. New diamond tooling-based production methods have been introduced, allowing for faster, more accurate, and cheaper task completion.[130] Toolmakers have also been paying more and more attention to the tool fabrication processes. In China, with its synthetic diamond production of over 20 billion carats annually, accounting for more than 80% of the world's total production,[131] the high-pressure, high-temperature sintering technology has produced diamond-impregnated segments for drilling and sawing in a lab setting.[132]

3D printing is a powerful technology to manufacture parts layer by layer using computer-aided design, and it has emerged recently as a key area of research in tool development. Yang et al. reported the 3D manufacturing of dental ceramic tools with neatly organized abrasive diamond particles (>100 µm) using laser sintering technology, which offered good cost/performance ratios and straightforward manufacturing procedures.[111] The 3D dispersion of the sizeable diamond particles was made more uniform by using laser rapid scanning, which greatly enhanced the manufacturing performance of the grinding wheels. Cr carbides were generated at the surface of the diamond particles, which improved the bonding strength between the Ni–Cr alloy matrix and abrasive diamond particles. Consequently, the dia-

© 2025 The Author(s). Advanced Materials Technologies published by Wiley-VCH GmbH

2365709x, 2025, 22, Downloaded from https://advanced.onlinelibrary.wiley.com/doi/10.1002/admt.202501111, Wiley Online Library on [19/11/2025]. See the Terms and Conditions (https://onlinelibrary.wiley.com/terms-and-conditions) on Wiley Online Library for rules of use; OA articles are governed by the applicable Creative Commons License

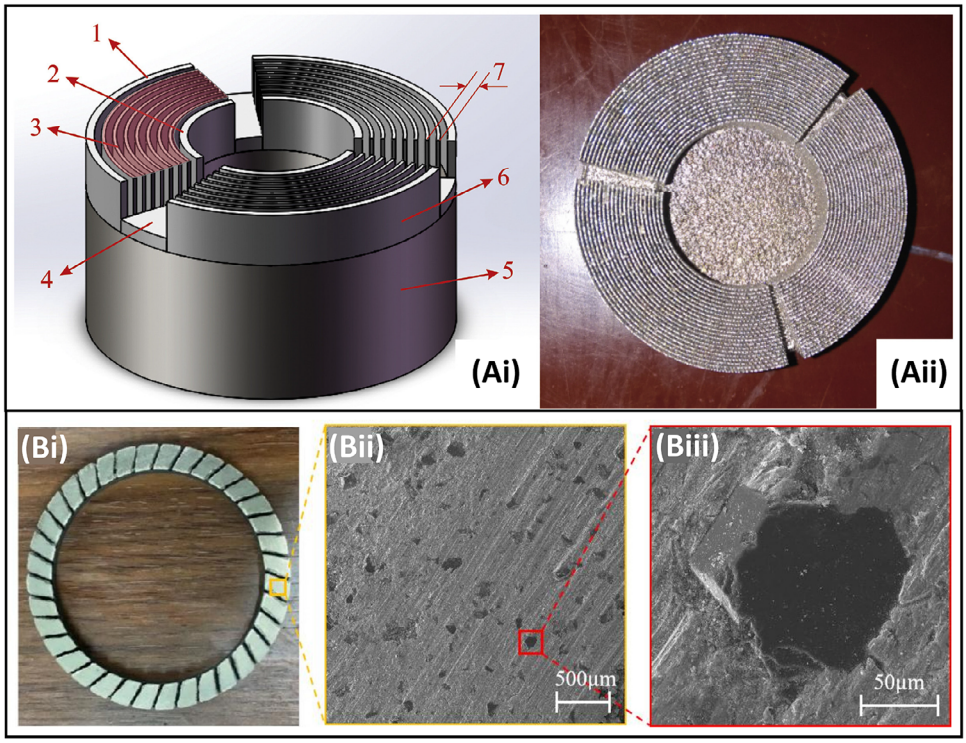


Figure 9. A) 3D printed diamond-impregnated bit with grid-shaped matrix fabricated using laser beam PBF technology: Ai) the design and Aii) as-printed working layer. Labels in Ai): 1 – grid piece on the outside, 2 – grid piece on the inside, 3 – grid pieces in the middle, 4 – waterways, 5 – steel body, 6 – matrix, 7 – space between two adjacent grid pieces. Reproduced with permission from ref. [133]. Copyright 2020, Elsevier. B) 3D printed diamond grinding wheel prepared using dual-filament technology: Bi) top-view image of the working layer after dressing with the linear cooling channels well visible, Bii) matrix surface morphology of the yellow region, and Biii) microscopic morphology of a single diamond particle. Reproduced with permission from ref. [110]. Copyright 2024, Springer.

mond particles demonstrated adequate wear and fracture resistance, with no falling-off cases noticed under heavy-load grinding conditions (i.e., tool speed 1200 m min^{-1}, workpiece speed 1 m min^{-1}, depth of cut 0.05 mm) against zirconia ceramic (ZrO_2).

With the increasing worldwide demand for mineral resources and the development of mineral exploration, deep ore prospecting still represents a major mining industry. So far, drilling is the critical cost factor, and impregnated diamond bits are the main tools for resource extraction and geological exploration. In this perspective, Wu and co-workers presented the manufacture of diamond-impregnated bits with a grid-shaped matrix (DIBGM) using 3D printing technology to improve the drilling efficiency in hard rock formation.[133] They used a 3D printer with laser beam PBF technology to produce the DIBGM with a steel body and radial concentric grid pieces distributed throughout the working layer of the bit matrix (see **Figure** 9A). A mixture feedstock of Co-Cr-Mo alloy and diamond powders was used in their DIBGM design with a diamond concentration of 2–4%. Compared to the traditional impregnated diamond bits, the DIBGM provided a 67% larger calculated specific pressure of 113 kgf cm^{-2} on the bottom surface lip. Additionally, rock cutting tests conducted by using a precision microtome and two 3D-printed grid pieces demonstrated high machining efficiency in hard rock formations (sandstone, slate, and granite).[133]

Diamond tools are also indispensable in the machining of other very hard materials such as ceramics and cemented carbide (WC-Co), which particularly present significant challenges due to their high hardness, strength, and excellent wear resistance. Comparatively little research has been done on diamond grinding heads made especially for hole processing and grooving of cemented carbide. Moreover, the conventional techniques for producing diamond grinding heads, such as hot-pressing sintering, brazing, and electroplating, have drawbacks when creating double-layer structures. These issues include uneven diamond particle sedimentation, high scrap rates, and the inability to precisely control diamond particle placement. Recently, though, a novel double-layer diamond grinding head specifically designed for grooving cemented carbide was fabricated using dual-nozzle FDM 3D printing technology.[108] The printed green body underwent post-processing, including thermal degreasing, hot pressing, sintering, and dressing. Seeking maximized abrasive utilization, reduced raw material waste, and minimized production costs, the design featured diamond particles exclusively on the outer wall. Particularly, grinding heads were produced with different diamond concentrations (5–25 vol.%), particle sizes (25–250 μm), and cobalt content (0–16 vol.%). Grinding experiments carried out on cemented carbide showed that the diamond particle size has the most pronounced effect, with a smaller diamond particle size lowering both the mechanical properties and wear resistance, as well as grinding efficiency, despite the favorable lower surface roughness post-grinding.

© 2025 The Author(s). Advanced Materials Technologies published by Wiley-VCH GmbH

2365709x, 2025, 22, Downloaded from https://advanced.onlinelibrary.wiley.com/doi/10.1002/admt.202501111, Wiley Online Library on [19/11/2025]. See the Terms and Conditions (https://onlinelibrary.wiley.com/terms-and-conditions) on Wiley Online Library for rules of use; OA articles are governed by the applicable Creative Commons License

In another study, a novel type of diamond grinding wheel with linear cooling channels was prepared by using dual-filament 3D printing technology.[109,110] The raw materials for the 3D printing included two different powder mixtures, namely i) CuSn15 alloy powder, diamond powder (30–150 μm), and a binder composed of high-temperature resistant resin, thermoplastic elastomer and polyolefin for the working layer and ii) alumina powder, graphite powder, and a binder consisting of high-temperature resistant resin, thermoplastic elastomer, polyolefin and surfactant for the flow channel, respectively. Optical and electron microscopy images of the diamond grinding wheel (Figure 9B) show an even distribution of diamond particles deeply embedded within the matrix. Grinding experiments conducted on four types of hard and brittle materials (i.e., red sandstone, concrete, alumina ceramic plate, and optical glass) demonstrated superior grinding performance over that of conventional dense grinding wheels without channels.[110] Furthermore, the grinding performance of the 3D printed diamond grinding wheel was found to be positively correlated with the volume concentration and grain size of the diamond filler.[109]

Copper-tin-diamond composite manufacturing was explored by using FDMS technology.[134] Sample morphological analysis revealed increased porosity within the composite with increased concentration of diamond particles, resulting in decreased relative density, bending strength, and holding ability. The particle agglomeration was affected by the diamond particle size, with finer particles corresponding to more severe particle agglomeration, potentially leading to the generation of cavities in the sample as well as reduced overall material performance. Ultra-thin dicing blades were successfully manufactured by wire cutting and thinning out of selected post-processed composites comprising Cu-Sn15 matrix powder, diamond particles (20–44 μm), and binder with thermoplastic elastomer and modified polyolefin. In a follow-up study, two different binder systems were used to fabricate the metal-based diamond composites.[135] Samples printed using thermoplastic-based binder presented a more uniform microstructure and obtained better flexural strength and relative density compared with composites prepared with paraffin-wax-based binder.

A recent example of the versatility of additive manufacturing to fabricate lightweight, high-performance materials with intricate geometry was reported by Kraiem et al.[136] They employed laser powder bed fusion to successfully manufacture parts of dense (97%) AlSi10Mg, augmented with 5 vol.% diamond. Crack-free metal matrix composites (MMCs) were produced from uncoated diamond particles (mean diameter of 25 μm) added to spherically shaped AlSi10Mg (size range of 15–45 μm). Despite partial graphitization of the diamond during the process, the density and mechanical properties of printed MMCs were still higher after diamond addition. This was ascribed to a direct interfacial reaction and aluminium carbide formation between the molten aluminium and the diamond reinforcement. The effect of diamond grain size on the formability and mechanical properties of 3D printed metal-bonded diamond tools based on the same AlSi10Mg matrix was studied by Tian et al.[137] Selective laser melting (LSM) of AlSi10Mg powder (15–53 μm) and five different diamond powders of varying mesh (particle diameter varying in the range 25–75 μm) resulted in the diamond abrasives being evenly distributed and firmly embedded into the metal binder with chemical metallurgical bonding. However, with fixed diamond volume fraction, a decrease in the diamond grain size was found to lower the relative density and main mechanical properties of the printed parts, including Young's modulus, compressive strength, tensile strength, yield strength, flexural modulus, and flexural strength.

Laser-based DED was employed by Chen et al. to 3D print Ti6Al4V/diamond MMCs.[138] Without premixing the powders with designated Ti6Al4V and diamond particle sizes of 45–106 and 53–63 μm, respectively, high diamond loadings (up to 50 wt.%) were applied. Enhanced thermal conductivity and mechanical strength were found with an increase in the diamond loading. With a nominal diamond loading of 40 wt.%, a two-fold improvement of the thermal conductivity was obtained, compared to Ti6Al4V. However, a higher amount of defects and porosity led to a drop in mechanical properties and thermal conductivity at relatively high loading. Overall, peak values for compression strength and modulus were found for diamond loadings in the range of 20–30 wt.%. According to the authors, these 3D printed metal matrix composites with improved thermal and mechanical properties show a high potential in space applications (e.g., spacecraft radiators, aircraft electronic racks) and as biomedical devices (e.g., medical implant material). Fang et al. fabricated metal matrix diamond composites by SLM in an argon-gas-filled working chamber at different forming parameters.[139] Particularly, they used metal (Ni10Co10Cu40Sn9Fe31) powder with an average size of 48 μm, diamond particles with an average size ≈200 μm, and a diamond concentration of 20 vol.%. Compared to MMCs created by vacuum brazing and hot-pressing sintering, the diamond particles in the SLM-formed composites were fixed by the metal matrix more firmly and with lower thermal damage.

Additive manufacturing technology provides unique opportunities for the production of functionally graded materials (FGMs) by stacking materials layer-by-layer and thus enabling diamond-based tool products with spatially varying mechanical properties. Rahmani et al. explored the 3D printing of mixed Ti6Al4V and diamond powders by SLM and introduced a combination of SLM and spark plasma sintering to incorporate diamond particles into various 3D-built metallic structures. They fabricated parts for use as tunnel boring cutters and mining equipment blades. Through a series of studies[140–142] involving impact-abrasive laboratory experiments and finite element modelling, they showed that functionally graded lattice structures composed of Ti6Al4V and stainless steel AISI 316L allowed an accurate distribution of diamond particles across them. In particular, the use of Ni-coated diamond particles, with various types and average grain sizes tested in the range from 6 to 50 μm, resulted in higher homogeneity of distribution of diamond in the composites after sintering as compared to pure polycrystalline diamond powder.[140] In terms of tribological performance, increased ductility and higher impact-abrasive resistance of the composites were reported with the addition of a higher content of coated diamond particles. Recently, Kong et al. reported diamond/cemented carbide FGMs produced via filament-based material extrusion 3D printing combined with high-temperature and high-pressure synthesis.[143] They specially designed FGMs to realize a gradient transition from cemented carbide to diamond by a systematic variation in diamond particle (20–30 μm) concentration along the building direction, applying eight gradient layers and matching filaments.

© 2025 The Author(s). Advanced Materials Technologies published by Wiley-VCH GmbH

2365709x, 2025, 22, Downloaded from https://advanced.onlinelibrary.wiley.com/doi/10.1002/admt.202501111, Wiley Online Library on [19/11/2025]. See the Terms and Conditions (https://onlinelibrary.wiley.com/terms-and-conditions) on Wiley Online Library for rules of use; OA articles are governed by the applicable Creative Commons License

Material samples without visual surface defects were synthesized at 6.5 GPa and 1550 °C. Analysis revealed that a gradient composition change optimized the bonding strength and residual stress from a mismatch of the coefficient of thermal expansion, as compared with a conventional polycrystalline diamond compact. Also, a 15% increase in impact resistance was recorded in drop-weight tests. Although further research is required to optimize the gradient design and performance of diamond/cemented carbide FGMs, it is evident that the filament-based material extrusion technology holds great potential in the development of high-performance FGMs in mass production.

The 3D printing of diamond-resin composites is another route to diamond tool production that has gained research attention recently. Meng et al. prepared UV-curable diamond/resin slurries with micron-sized diamond powder and used DLP for the preparation of composite specimens that were subjected to various mechanical and thermal analyses.[144,145] Slurries containing non-treated diamond powders with particle sizes of 15–20 µm and solid contents ranging from 6.25 to 25 vol.% were successfully printed.[144] The slurry viscosity increased with the diamond content, yet for all investigated slurries, it was found suitable for printing with DLP technology. The cure depth and cure width decreased with an increase in diamond loading, while the thermal stability of printed specimens improved with it, according to thermogravimetric analysis. Three-point bending tests demonstrated that the flexural strength of printed bar-shaped specimens decreased from 40.0 to 23.9 MPa for diamond contents ranging from 0 to 18.75 vol.%, and it levelled off with further increase to 25 vol.%. Generally, the poor bonding condition between diamond powder and resin matrix is a challenging problem. To provide an effective solution for such composites, Yang et al. showed that the coating of the diamond particles with Al_2O_3 via a hydrothermal-assisted chemical precipitation method improves the interfacial adhesion.[145] They reported improved oxidation resistance and reduced UV light absorbance of the coated diamond powder. Compared with the pristine diamond resin suspension, the coated diamond UV curable resin suspension showed higher viscosity and suspension stability. In addition, the Al_2O_3 coating led to improved mechanical response of the DLP processed diamond-resin composite, including ≈36% increase in the bending strength and ≈26% increase in the elasticity modulus. Phenolic resin-based diamond tool parts with controllable porosity and structure were successfully prepared by 3D gel-printing (extrusion) by Shao et al.[146] This rapid prototyping technology, developed on the basis of gel molding, has the advantages of low cost and high solid content, and has promising future applications in the field of manufacturing tailored abrasive materials. Specifically, the authors used two kinds of sharp-edged diamond powders with median diameters of 1.58 and 2.61 µm, respectively, to 3D gel-print a variety of bar-shaped parts. The three-point bending strength of dense printed parts was ≈23.7 and 27.0 MPa, while for the porous printed parts (porosity 20–5%), it monotonically decreased from 18.2 to 11.8 MPa and from 21.6 to 15.5 MPa, respectively.

Additive manufacturing via DLP of SiC ceramics is commonly hampered by the low solid content of the photosensitive slurry, leading to high residual Si content and low strength of the printed parts. By introducing quasi-spherical diamond powder (D_{50} = 13.5 µm) as the high-density carbon source, Tang et al. managed to effectively improve the printing properties, such as the curing thickness, viscosity, and stability of the slurries.[147] High-strength reaction-bonded SiC components with complex structure were successfully produced through DLP-based 3D printing technology combined with reactive melt infiltration. The final samples exhibited an elastic modulus of 359.16 ± 4.57 GPa and a specific flexural strength of 312.45 ± 18.75 MPa, which are among the highest values reported for 3D-printed SiC composites.

Chen et al. investigated SLA-based 3D printing to manufacture grinding wheels from a vitrified bond and diamond (10 ± 5 µm) slurry system (involving silane coupling agents) with high solid content, low viscosity, and good stability.[107] Complex-shaped gyroid triply periodic minimal surface grinding wheels were fabricated, and their grinding performance (removal rate, grinding temperature, and surface roughness) was tested against SiC ceramic and compared to that achieved using a conventional solid structure grinding wheel. The gyroid porous grinding wheel showed better self-sharpening and achieved a lower surface roughness (0.069 µm vs 0.155 µm) and 27% lower grinding temperature of 106 °C.

The chemical stability and efficient heat conduction of diamond make diamond powder a highly attractive additive to achieve green manufacturing when combined with advanced manufacturing techniques. To this purpose, Tang and Tang successfully 3D printed functionally graded diamond/geopolymer composites with self-healing ability at room temperature and good thermal stability via extrusion-based additive manufacturing.[148] They formulated two different inks using alkaline potassium silicate, dry geopolymer, and diamond powder (0 and 15 wt.% diamond) and chose titanium-plated diamond (3.5–4.2 µm) to avoid graphitization. The addition of diamond could avoid the occurrence of cracks during high-temperature conditions up to 1200 °C due to its excellent thermal conductivity. Promoted thermal repair was demonstrated, and the aggregation and growth of an emission-like secondary mullite phase on the original mullite phase were seemingly caused by heat preservation of diamond and the decrease in crystallization temperature.

4.5. Biomedical Engineering

Diamond is a suitable material in a quickly growing number of biomedical applications, such as bone[149] and tissue implants, tissue engineering scaffolds,[62] bioimaging and theranostics,[150] anti-cancer therapy,[151] drug[49] and gene delivery, and antimicrobial agents.[152] Particularly, NDs provide a unique combination of properties that render them superior to other nanomaterials. These distinct features include their small size (≈5 nm), scalable production and low cost, negligible toxicity, chemical inertness of the bulk diamond core linked to a rich chemistry of the surface, and bright and robust fluorescence resistant to photobleaching.[62,153] The direct printing of NDs, as well as their incorporation into composites and hybrid materials, followed by the 3D printing of diamond-based structures and platforms, are emerging research areas in biology and medicine.

A relatively early proof-of-concept study of the 3D printing of variously shaped objects using a layer-by-layer additive manufacturing method was reported by Angjellari et al.[154] They used

© 2025 The Author(s). Advanced Materials Technologies published by Wiley-VCH GmbH

2365709x, 2025, 22, Downloaded from https://advanced.onlinelibrary.wiley.com/doi/10.1002/admt.202501111, Wiley Online Library on [19/11/2025]. See the Terms and Conditions (https://onlinelibrary.wiley.com/terms-and-conditions) on Wiley Online Library for rules of use; OA articles are governed by the applicable Creative Commons License

dispersions of poly(vinyl alcohol) (PVA) and DNDs to produce PVA-DND nanocomposites representing an innovative material class for stable and biocompatible systems (e.g., scaffolds). Significant enhancement in the hardness and indentation modulus was noticed with respect to the pure PVA material, even with small additions of DND (from 0.5% w w^{-1}).

In 2020, Fox et al. described the fabrication of diamond-based implant materials using laser cladding technology to 3D print a composite of 50 µm diamond powder and fused titanium material, a common medical implant material.[155] Composite scaffolds of up to 50% diamond were successfully produced while the diamond content remained capable of typical diamond fluorescence as imaged by confocal microscopy. The incorporation of diamond made the scaffolds more hydrophilic and improved the cell viability (adhesion and proliferation) of Chinese Hamster Ovarian (CHO) cells. In a subsequent study, Mani et al. reported the feasibility of fabricating diamond–titanium hybrid electrodes for neuronal interfacing using laser metal deposition.[156] The behavior of the printed planar material was influenced by various parameters, such as powder chemistry (micro-diamond content), surface functionalization (oxygen plasma), and morphology (surface roughness). With a 50% diamond volume fraction, the electrodes exhibited a high electrochemical capacitance of 1.1 mF cm^{-2} and a low electrochemical impedance of 1 kΩ cm^2 at 1 kHz in physiological saline. Furthermore, they exhibited a high degree of biocompatibility assessed in vitro using cortical neurons. The core team of researchers recently reported the 3D printing of biocompatible titanium-diamond composite structures for implant applications using laser metal deposition.[157] Parts were fabricated comprising 30% and 50% diamond, and experimentally determined values of the hardness, ultimate tensile strength, and yield strength were 4–6 GPa, 426 MPa, and 375 MPa, respectively. Increasing the diamond composition to 30% led to higher osteoblast viability and lower bacteria count compared with titanium. The manufacturing approach was finally argued as a potential route to patient-specific diamond implant solutions.

In another work, a stamping method for designing and fabricating a diamond platform for ordered neural cell adhesion was shown.[78] Herein, µCP was used for patterned ND seeding, and CVD was conducted subsequently to form thin-film polycrystalline diamond arrays with square patterns of ≈50 × 50 $µm^2$. The PDMS stamp was fabricated by casting on a micro-patterned silicon substrate, which was first developed using conventional optical lithography. From earlier work, it was already concluded that rat cortical neurons survived on the polycrystalline diamond as used here in the patterned growth of diamond in significantly higher densities than on tissue culture plastic after 24 h of incubation.[158]

Digital dentistry can benefit from the unique features of NDs when embedded in the biomaterial used for 3D printing. Polymer-based 3D-printed dental appliances, such as orthodontic attachments, brackets, and provisional crowns, lack strength and hardness and, as a result, require frequent replacement due to surface damage or loss of structure. In a microbial-rich oral environment, such limiting physicochemical factors enable biofilm formation and bacterial attachment. Mangal et al. showed that NDs, which are known for their exceptional strength, high modulus, and biocompatibility, can significantly enhance the bulk properties of PMMA, a synthetic thermoplastic polymer, even at a very low concentration of 0.1 wt.%.[159,160] They used solution-based mixing with the aid of a high-power sonication probe in combination with magnetic stirring to incorporate pure non-functionalized NDs and amine-functionalized NDs into the PMMA (**Figure 10A**). Following, custom-designed cuboidal specimens were printed with a DLP 3D printer. Statistically significant increase in the Vickers micro-hardness ($p < 0.001$) was revealed in the nanocomposites, along with enhanced resistance to surface loss ($p < 0.001$) in comparison to the unfilled PMMA for both stainless steel and titanium countersurfaces.[159] Although both nanocomposites showed markedly improved mechanical properties, the aminated ND-containing composite showed higher flexural strength, impact strength, and elastic modulus compared to the control and ND-containing specimens, which was ascribed to stronger covalent linkages and the somewhat better monodisperse state of the aminated NDs in the polymer.[160] Compared to the unmixed PMMA, both the ND-containing nanocomposites exhibited significantly enhanced resistance to the formation of *Streptococcus* mutant biofilms after 48 h ($p < 0.01$). The confocal imaging of the bacterial biofilm revealed distinctive biofilm thickness (Figure 10Bi) and biomass (Figure 10Bii), with the highest values derived on the control group and statistically significantly lower numbers on both the ND-variant nanocomposites ($p < 0.01$). Insignificant differences in the biofilm thickness and biomass were found between the ND-incorporated and aminated ND-incorporated variants.[159] Finally, with the ultimate aim of fabricating orthodontic customized appliances with high quality of fit, the accuracy of 3D-printed orthodontic brackets made using the (aminated) ND-nanocomposites was confirmed using trueness analysis.[160] A morphometric comparison, with deviations of ±200 µm and tolerances of ±10 µm assigned, verified the absence of any significant morphological changes in printing accuracy due to incorporation of (aminated) NDs. Although the studies were conducted in vitro and the findings must be verified in vivo, the reported ND-filler approach provides a promising solution to tackle the challenge of the intra-oral aging of 3D-printed appliances due to microbial insult.

4.6. Other Applications

Further application domains and potential use cases of 2D and 3D printed diamond include electronics, optics, and quantum physics. Already in 2011, Zhang et al. developed a diamond paste by mixing ND powder with nanocrystalline graphite and ethyl cellulose, which was subsequently applied in screen printing to fabricate low-cost and large-area nanodiamond film electron emission cathodes.[72] A three-step thermal sintering process was used to remove organic material and to fix the nanodiamond film on the substrates. Following, a hydrogen plasma post-treatment was applied to improve the field emission stability and uniformity of the screen-printed films, characterized by a turn-on field of 1.25 V $µm^{-1}$. According to the authors, this plasma treatment made the nanodiamond emission tips sharper and their distribution more uniform, and enabled electrons to tunnel in the film. However, little information was given on the number of dark/dead pixels in the high-density films. Also, a minimum average distance between the nanodiamond emitters required to limit

© 2025 The Author(s). Advanced Materials Technologies published by Wiley-VCH GmbH

2365709x, 2025, 22, Downloaded from https://advanced.onlinelibrary.wiley.com/doi/10.1002/admt.202501111, Wiley Online Library on [19/11/2025]. See the Terms and Conditions (https://onlinelibrary.wiley.com/terms-and-conditions) on Wiley Online Library for rules of use; OA articles are governed by the applicable Creative Commons License

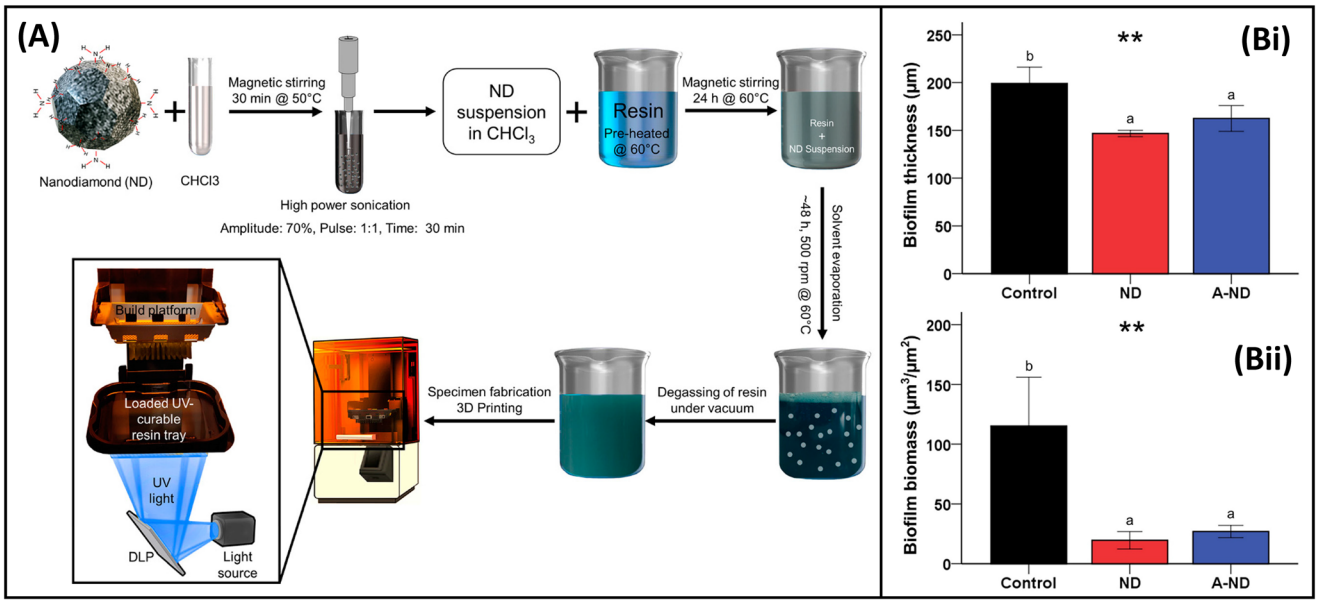


Figure 10. A) Depiction of the process used to prepare and manufacture nanocomposites of biological-grade and UV-curable acrylate-based resin material (PMMA) and NDs as nanofiller. Specimens were fabricated using a DLP 3D printer with polymerization under 405 nm light and post-processing using a UV oven. Reproduced with permission from ref. [160]. Copyright 2020, MDPI. B) Quantitative analysis of the biofilm thickness Bi) and biomass Bii) attached on the surfaces of control (without ND filler) and non-functionalized NDs (ND) and amine-functionalized NDs (A-ND) incorporated nanocomposite. *Streptococcus* mutants (*S. mutants*, ATCC 25175) strain was used in the experiment. The lowercase letters above the error bars indicate significant differences. $^{**}p < 0.01$ for the comparison between the groups. Reproduced with permission from ref. [159]. Copyright 2020, Elsevier.

interactions or screening electronic field effects was not reported. Potential use of the as-produced film cathode was argued for future military electronic devices and outdoor displays, although it has to be noted that the technology of field-emission cathodes fabricated from synthesized CNTs or suspensions of CNTs (e.g., screen printing) is far more advanced. Leading consumer electronics companies like Samsung, Sony, and Philips had worked on the development of this kind of display, but the research and commercialization stopped ≈2010 because of the emergence of the organic light-emitting diodes (OLEDs).[161]

Nahlik et al. developed single- and double-layered UV photodetectors via a sequential inkjet printing on an interdigitated electrode platform using diamond and zinc oxide precursor inks.[89] In particular, the nanodiamond ink was prepared from a dispersion of DNDs and ethylene glycol (400 mg L^{-1}). At a wavelength of 365 nm, the photoresponsivity of the double-layered photodetector (ZnO/ND) was 0.35 A W^{-1}, providing more than 10 times higher response and faster reactivity in comparison to the single-layered photodetector (ZnO) from 30 to 90 °C. From a preliminary attempt to improve the optical properties of polymeric acrylate resin by incorporation of microdiamond powder (median grain diameter of 125 nm), Kowalewska et al. anticipated the effective production and future application potential of such diamond-polymer composites in 3D-printed optical elements.[162]

A myriad of different color centers, i.e., fluorescent crystallographic defects embedded within the crystal lattice, have been identified in diamond.[163,164] Owing to their unique quantum properties and robustness even at room temperature, the quantum defects in NDs, such as the nitrogen-vacancy (NV) centers, offer a viable path to the realization of multiple upcoming quantum technologies, e.g., spintronics, data storage, quantum optics, quantum computing, and quantum sensing.[165] For many of the practical applications, the controlled placement (or embedding) of NDs with respect to target sites is essential. For this purpose, Xu et al. developed an electrohydrodynamic dispensing method to print NDs (≈40 nm sized, carboxylated surface, 1–4 NVs per particle) directly on common substrates like silicon and glass.[90] By configuring a glass nanopipette to a printer head with a three-axis positioning stage, they established a high-precision printing process with on-demand control over the quantity (including single-particle level) and position of printed NDs in arbitrary patterns (**Figure 11**). This lithography-free, direct printing approach was shown to be flexible and accurate, and it could be extended for printing fluorescent NDs of various sizes and defect densities and types (e.g., SiV^- centers) for their implementation into diverse fields. Regarding diamond-based quantum computing and communication, however, it is questionable whether this quantum defect placement approach will be able to compete with the other developed techniques to precisely position and activate individual defects in diamond using focused ion beams.

5. Conclusion and Outlook

Diamond particle printing has developed into a vibrant field of materials research that makes it possible to create structures and functions that are difficult to achieve with traditional manufacturing techniques. Diamond powders are available in a wide range of particle sizes, from a few nanometers up to hundreds of microns, and are produced synthetically at consistent quality and decreasing cost. They offer great processability with additive manufacturing owing to their small size, unique surface chemistry, and

© 2025 The Author(s). Advanced Materials Technologies published by Wiley-VCH GmbH

2365709x, 2025, 22, Downloaded from https://advanced.onlinelibrary.wiley.com/doi/10.1002/admt.202501111, Wiley Online Library on [19/11/2025]. See the Terms and Conditions (https://onlinelibrary.wiley.com/terms-and-conditions) on Wiley Online Library for rules of use; OA articles are governed by the applicable Creative Commons License

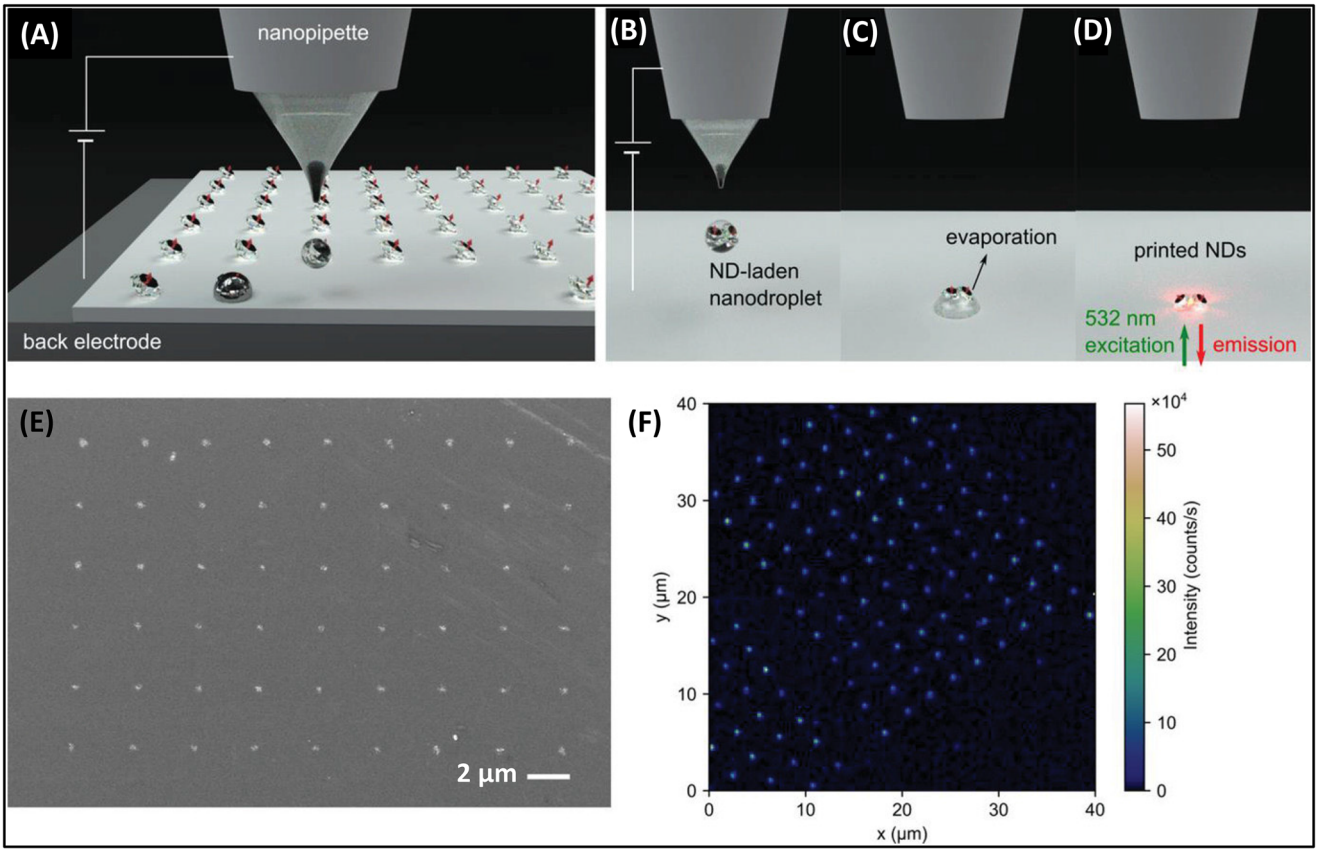


Figure 11. Inkjet-printing of fluorescent NDs. A) Concept sketch illustrating the electrohydrodynamic printing of NDs when a negative DC voltage is applied to a back electrode. The printing involves three steps: B) A nanodroplet containing NDs is ejected; C) The nanodroplet lands on the substrate and the solvent (deionized water) evaporates; D) Eventually, a cluster of NDs is formed, and the embedded NV centers are optically accessible. E) SEM image of an array of clusters with a 3 µm pitch (scale bar: 2 µm). F) Confocal fluorescence image of the printed array of ND clusters under 532 nm excitation (recorded fluorescence wavelength range: 647–800 nm). Reproduced with permission from ref. [90]. Copyright 2022, Wiley.

dispersibility in various liquid and solid media. The rapid development of printing technologies has created new opportunities for producing increasingly sophisticated and innovative diamond-based materials and devices with advanced functionality, performance, and continued miniaturization.

As demand grows for compact, high-performance technologies across the biomedical, sensing, and electronics sectors, printed diamond-based materials offer unique advantages in combining thermal management, chemical stability, and, in the case of BDD, electrical conductivity. Ink-based printing enables the precision engineering of diamond structures on a microscale. Successful fabrication of high-quality MEMS cantilevers and micro-resonators for mass and gas sensing has been demonstrated. Printable BDD electrodes support the rapid prototyping of robust and sensitive electrochemical sensors for environmental monitoring, biosensing, and healthcare. Also, 3D printing presents a viable path to the development of electrochemical and humidity sensors with a customizable flexible/stiff matrix and real-time monitoring capabilities. The 3D printing of diamond-based implant materials and dental appliances shows great promise for durable and patient-specific solutions. A major research activity is the 3D printing of diamond machining tools with ceramic, metal, or resin matrix materials. Novel diamond tooling production methods have been introduced for the fabrication of impregnated diamond bits, grinding wheels, and mining parts.

The rapid tooling of diamond-reinforced metal matrix composites provides highly satisfactory results in a bulk print. However, printed structures with intricate geometry can suffer from a relatively poor connection of metal struts due to weak bonding between diamond and metal matrix, causing brittle scaffold structures, for example. Further, diamond microparticles are reported to accumulate at the bottom of printed features due to differences in shape, size, weight, and density of diamond and matrix powders, respectively. To meet the growing quality demands, one of the crucial steps in the additive manufacturing involving diamond powders is particle size classification. In many studies, the description of the materials' characteristics of the diamond powders employed is rather limited. Yet, the powders must be very precisely specified for size, shape, and also composition to ensure both the optimal density of diamond particles within the matrix and compatible interfacial mechanical properties. Also, more attention should be paid to the surface functionalization and modification of the diamond powders to make them fit for the printing process and desired application. This could include oxidation, hydrogenation, or

© 2025 The Author(s). Advanced Materials Technologies published by Wiley-VCH GmbH

2365709x, 2025, 22, Downloaded from https://advanced.onlinelibrary.wiley.com/doi/10.1002/admt.202501111, Wiley Online Library on [19/11/2025]. See the Terms and Conditions (https://onlinelibrary.wiley.com/terms-and-conditions) on Wiley Online Library for rules of use; OA articles are governed by the applicable Creative Commons License

graphitization, to improve their chemical and physical properties, and the grafting of specific groups or function-guidance molecules (coupling agents) to provide covalent bonding between NDs and polymer/resin matrix, and improved uniformity of particle distribution. By adding a high-temperature resistant and weldable metallization layer to diamond powder surfaces, the bonding strength between diamond and matrix in diamond tools can be effectively enhanced, and it provides protection against diamond oxidation. Surface coating techniques like fluidized-bed atomic layer deposition to produce core-shell composite diamond powders with highly conformal metal (oxide) nanolayers hold great promise.

For optimum diamond printing performance, regardless of the end application, an interdisciplinary expertise from the involved researchers is essential. The material characteristics of the applied diamond powders, as well as the printing design, processing, and apparatus configuration, need to be optimized to achieve the maximum potential, something that is not always apparent in the relatively young but quickly growing practice of diamond particle printing. Adaptation of printing hardware to handle the abrasive nature of diamond particles is critical for practical implementation. This includes custom nozzles, hardened feeding systems, and wear-resistant components, particularly in FDM and extrusion-based systems. Standardization and scaling will be essential for translating these technologies from lab-scale demonstrations to industrial applications. This includes establishing benchmarks for performance, durability, and compatibility across different printing platforms.

Looking ahead, the integration of artificial intelligence and machine learning presents a powerful opportunity to accelerate research and development in diamond particle printing. Data-driven models can support the rational design of ink formulations, optimize print parameters, and predict structure-property relationships, significantly reducing experimental workload. As the cost of synthetic diamond continues to decline and additive manufacturing technologies become more accessible and precise, the prospects for printed diamond-based materials and devices are brighter than ever.

Supporting Information

Supporting Information is available from the Wiley Online Library or from the author.

Acknowledgements

S.B. gratefully acknowledges the support of the Charles University Primus program (Grant No. PRIMUS/25/SCI/020).

Conflict of Interest

The authors declare no conflict of interest.

Keywords

additive manufacturing, diamond particles, functional composite materials, (micro) fabrication, multiscale

Received: May 26, 2025
Revised: July 11, 2025
Published online: August 12, 2025

[1] R. S. Balmer, J. R. Brandon, S. L. Clewes, H. K. Dhillon, J. M. Dodson, I. Friel, P. N. Inglis, T. D. Madgwick, M. L. Markham, T. P. Mollart, N. Perkins, G. A. Scarsbrook, D. J. Twitchen, A. J. Whitehead, J. J. Wilman, S. M. Woollard, *J. Phys. Condens. Matter* **2009**, *21*, 364221.
[2] Y.-J. Lu, C.-N. Lin, C.-X. Shan, *Adv. Opt. Mater.* **2018**, *6*, 1800359.
[3] R. Zulkharnay, P. W. May, *Functional Diamond* **2024**, *4*, 2410160.
[4] S. Koizumi, C. Nebel, M. Nesladek, *Physics and Applications of CVD Diamond*, Wiley, Weinheim, Germany **2008**.
[5] N. Yang, S. Yu, J. V. Macpherson, Y. Einaga, H. Zhao, G. Zhao, G. M. Swain, X. Jiang, *Chem. Soc. Rev.* **2019**, *48*, 157.
[6] M. L. Hicks, A. C. Pakpour-Tabrizi, R. B. P. Jackman, *Diam. Relat. Mater.* **2019**, *97*, 107424.
[7] B. Ali, I. V. Litvinyuk, M. F. L. M. D. Rybachuk, *Carbon* **2021**, *179*, 209.
[8] J.-C. Arnault, S. Saada, V. Ralchenko, *Phys. Status Solidi – Rapid Res. Lett.* **2022**, *16*, 2100354.
[9] Z. Liu, S. Baluchová, A. F. Sartori, Z. Li, Y. Gonzalez-Garcia, M. Schreck, J. G. Buijnsters, *Carbon* **2023**, *201*, 1229.
[10] S. Feijoo, S. Baluchová, M. Kamali, J. G. Buijnsters, R. Dewil, *Environ. Pollut.* **2024**, *347*, 123705.
[11] A. Krueger, *J. Mater. Chem.* **2011**, *21*, 12571.
[12] S. Kumar, M. Nehra, D. Kedia, N. Dilbaghi, K. Tankeshwar, K.-H. N. Kim, *Carbon* **2019**, *143*, 678.
[13] V. N. Mochalin, O. Shenderova, D. Ho, Y. Gogotsi, *Nat. Nanotechnol.* **2012**, *7*, 11.
[14] A. E. Fischer, G. M. Swain, *J. Electrochem. Soc.* **2005**, *152*, B369.
[15] T. Kondo, *Chem. Lett.* **2021**, *50*, 733.
[16] T. Kondo, H. Sakamoto, T. Kato, M. Horitani, I. Shitanda, M. Itagaki, M. S.-P. D. E.: A. Yuasa, *Electrochem. Commun.* **2011**, *13*, 1546.
[17] T. Kondo, I. Udagawa, T. Aikawa, H. Sakamoto, I. Shitanda, Y. Hoshi, M. Itagaki, M. Yuasa, *Anal. Chem.* **2016**, *88*, 1753.
[18] S. Baluchová, S. van Leeuwen, B. Kumru, J. G. Buijnsters, *ACS Appl. Polym. Mater.* **2024**, *6*, 14638.
[19] C. Zhu, H. B. Gemeda, E. B. Duoss, C. M. T. M. Spadaccini, *Adv. Mater.* **2024**, *36*, 2314204.
[20] D. Wu, S. Wu, P. Narongdej, S. Duan, C. Chen, Y. Yan, Z. Liu, W. Hong, I. Frenkel, X. He, *Adv. Mater.* **2024**, *36*, 2307632.
[21] H. Wu, R. Luo, Z. Li, Y. Tian, J. Yuan, B. Su, K. Zhou, C. Yan, Y. Shi, *Adv. Mater.* **2024**, *36*, 2307546.
[22] D. Surana, *International Journal of Research Publication and Reviews* **2025**, *6*, 5842.
[23] R. S. Ruoff, *Carbon* **2018**, *132*, 802.
[24] D. Das, In *Carbon-Based Nanofillers and Their Rubber Nanocomposites*, (Eds: S. Yaragalla, R. Mishra, S. Thomas, N. Kalarikkal, H. J. Maria), Elsevier, Amsterdam, **2019**, pp. 123–181.
[25] M. Kiss, S. Mi, G. Huszka, N. Quack, *Adv. Opt. Technol.* **2021**, *10*, 19.
[26] J. Zhang, J. Wang, G. Zhang, Z. Huo, Z. Huang, L. Wu, *Mater. Des.* **2024**, *237*, 112577.
[27] J. Chen, Y. Zhu, J. Wang, Y. Peng, J. Yao, S. Ming, *Diam. Relat. Mater.* **2019**, *100*, 107595.
[28] D. Clematis, M. Panizza, *Curr. Opin. Electrochem.* **2021**, *30*, 100844.
[29] D. Kramer, *Phys. Today* **2022**, *75*, 22.
[30] M. B. Joseph, A. Colburn, T. P. Mollart, N. Palmer, M. E. Newton, J. V. Macpherson, *Sens. Actuator B-Chem.* **2017**, *238*, 1128.
[31] N. Nunn, M. Torelli, G. McGuire, O. N. Shenderova, *Curr. Opin. Solid State Mater. Sci.* **2017**, *21*, 1.
[32] S. Tagadiya, Introducing the Largest Lab Grown Diamond in the World: Pride of India **2023**. Available at:

© 2025 The Author(s). Advanced Materials Technologies published by Wiley-VCH GmbH

2365709x, 2025, 22, Downloaded from https://advanced.onlinelibrary.wiley.com/doi/10.1002/admt.202501111, Wiley Online Library on [19/11/2025]. See the Terms and Conditions (https://onlinelibrary.wiley.com/terms-and-conditions) on Wiley Online Library for rules of use; OA articles are governed by the applicable Creative Commons License

https://diamondrensu.com/blogs/lab-grown-diamonds/largest-certified-lab-grown-diamond-in-the-world-diamondrensu (accessed: August 2025).
[33] T. Yoshimoto, H. Yui, T. Iwata, *J. Vac. Sci. Technol. B:Nanotechnol.* **2010**, *28*, C2B30.
[34] M. S. Liliya, L. K. Elena, *Proc.SPIE* **2002**, *4767*, 90.
[35] G. P. Bogatyreva, G. A. Petasyuk, G. A. Bazalii, V. S. Shamraeva, *J. Superhard Mater.* **2009**, *31*, 126.
[36] J.-P. Boudou, P. A. Curmi, F. Jelezko, J. Wrachtrup, P. Aubert, M. Sennour, G. Balasubramanian, R. Reuter, A. Thorel, E. Gaffet, *Nanotechnology* **2009**, *20*, 235602.
[37] K. V. Volkov, V. V. Danilenko, V. I. Elin, *Combust. Explos. Shock Waves* **1990**, *26*, 366.
[38] Y. Guo-Wei, W. Jin-Bin, L. Qui-Xiang, *J. Phys. Condens. Matter* **1998**, *10*, 7923.
[39] M. Frenklach, W. Howard, D. Huang, J. Yuan, K. E. Spear, R. Koba, *Appl. Phys. Lett.* **1991**, *59*, 546.
[40] T. L. Daulton, M. A. Kirk, R. S. Lewis, L. E. Rehn, *Nucl. Instrum. Methods Phys. Res., B* **2001**, *175*, 12.
[41] É. M. Galimov, A. M. Kudin, V. N. Skorobogatskii, V. G. Plotnichenko, O. L. Bondarev, B. G. Zarubin, V. V. Strazdovskii, A. S. Aronin, A. V. Fisenko, I. V. Bykov, A. Y. Barinov, *Dokl. Phys.* **2004**, *49*, 150.
[42] A. Krüger, F. Kataoka, M. Ozawa, T. Fujino, Y. Suzuki, A. E. Aleksenskii, A. Y. Vul', E. Ōsawa, *Carbon* **2005**, *43*, 1722.
[43] O. Shenderova, N. Nunn, *Chapter 2 – Production and Purification of Nanodiamonds*, (Ed: J.-C. Arnault), Elsevier, Amsterdam, The Netherlands, **2017**, pp. 25–56.
[44] A. M. Schrand, H. S. A. Ciftan, O. A. Shenderova, *Crit. Rev. Solid State Mater. Sci.* **2009**, *34*, 18.
[45] Q. Zheng, X. Shi, J. Jiang, H. Mao, N. Montes, N. Kateris, J. A. Reimer, H. Wang, H. Zheng, *Proc. Natl. Acad. Sci. U.S. A.* **2023**, *120*, 2301981120.
[46] A. S. Barnard, M. Sternberg, *J. Mater. Chem.* **2007**, *17*, 4811.
[47] S. Turner *Chapter 3 – Structure, Shape, Defects and Impurities in Nanodiamonds Investigated by HRTEM and STEM-EELS*, In *Nanodiamonds*, (Ed: J.-C. Arnault), Elsevier, Amsterdam, The Netherlands **2017**, pp. 57–84.
[48] M. N. R. Ashfold, J. P. Goss, B. L. Green, P. W. May, M. E. Newton, C. V. N. D. Peaker, *Chem. Rev.* **2020**, *120*, 5745.
[49] Y. Tian, A. C. Nusantara, T. Hamoh, A. Mzyk, X. Tian, F. Perona Martinez, R. Li, H. P. Permentier, R. Schirhagl, *ACS Appl. Mater. Interfaces* **2022**, *14*, 39265.
[50] A. Morita, A. C. Nusantara, A. Myzk, F. P. Perona Martinez, T. Hamoh, V. G. Damle, K. J. van der Laan, A. Sigaeva, T. Vedelaar, M. Chang, M. Chipaux, R. Schirhagl, *Nano Today* **2023**, *48*, 101704.
[51] T. F. Segawa, R. Igarashi, *Prog. Nucl. Magn. Reson. Spectrosc.* **2023**, *134*, 20.
[52] H. J. Shulevitz, A. Amirshaghaghi, M. Ouellet, C. Brustoloni, S. Yang, J. J. Ng, T.-Y. Huang, D. Jishkariani, C. B. Murray, A. Tsourkas, C. R. Kagan, L. C. Bassett, *ACS Appl. Nano Mater.* **2024**, *7*, 15334.
[53] O. A. Shenderova, G. E. McGuire, *Biointerphases* **2015**, *10*, 030802.
[54] S. Heyer, W. Janssen, S. Turner, Y.-G. Lu, W. S. Yeap, J. Verbeeck, K. Haenen, A. Krueger, *ACS Nano* **2014**, *8*, 5757.
[55] J. Whitlow, S. Pacelli, A. Paul, *J. Contr. Release* **2017**, *261*, 62.
[56] I. C. Kuschnerus, H. Wen, X. Zeng, Y. Y. Khine, J. Ruan, C.-J. Su, U.-S. Jeng, H. A. Girard, J.-C. Arnault, E. Osawa, O. Shenderova, V. N. Mochalin, M. Liu, M. Nishikawa, S. L. Y. Chang, *Diam. Relat. Mater.* **2023**, *139*, 110199.
[57] A. Krueger, *J. Mater. Chem.* **2008**, *18*, 1485.
[58] S. Osswald, G. Yushin, V. Mochalin, S. O. Kucheyev, Y. Gogotsi, *J. Am. Chem. Soc.* **2006**, *128*, 11635.
[59] L. Ginés, S. Mandal, I. A. Ashek, C.-L. Cheng, M. Sow, O. A. Williams, *Nanoscale* **2017**, *9*, 12549.
[60] A. V. Shvidchenko, E. D. Eidelman, A. Y. Vul, N. M. Kuznetsov, D. Y. Stolyarova, S. I. Belousov, S. N. Chvalun, *Adv. Colloid Interface Sci.* **2019**, *268*, 64.
[61] M. Ozawa, M. Inaguma, M. Takahashi, F. Kataoka, A. Krüger, E. Ōsawa, *Adv. Mater.* **2007**, *19*, 1201.
[62] Y. Zamani, A. Zareein, L. Bazli, R. NasrAzadani, B. Pasha Mahammod, S. Nasibi, A. Modarresi Chahardehi, *J. Compos. Compd.* **2020**, *2*, 215.
[63] R. R. Suresh, M. Lakshmanakumar, J. B. B. Arockia Jayalatha, K. S. Rajan, S. Sethuraman, U. M. Krishnan, J. B. B. Rayappan, *J. Mater. Sci.* **2021**, *56*, 8951.
[64] Y. Zhang, Y. Zhu, S. Zheng, L. Zhang, X. Shi, J. He, X. Chou, Z.-S. Wu, *J. Energy Chem.* **2021**, *63*, 498.
[65] R. D. Crapnell, C. E. Banks, *ChemElectroChem* **2024**, *11*, 202400370.
[66] H. Zheng, Z. Guo, W. Zhu, D. Li, Z. Pu, *J. Adv. Manuf. Technol.* **2023**, *128*, 2813.
[67] T. Kondo, M. Horitani, H. Sakamoto, I. Shitanda, Y. Hoshi, M. Itagaki, M. Yuasa, *Chem. Lett.* **2013**, *42*, 352.
[68] T. Kondo, K. Nakajima, T. Osasa, A. Kotsugai, I. Shitanda, Y. Hoshi, M. Itagaki, T. Aikawa, T. Tojo, M. Yuasa, *Chem. Lett.* **2018**, *47*, 1464.
[69] T. Matsunaga, T. Kondo, T. Osasa, A. Kotsugai, I. Shitanda, Y. Hoshi, M. Itagaki, T. Aikawa, T. Tojo, M. Yuasa, *Carbon* **2020**, *159*, 247.
[70] T. Matsunaga, T. Kondo, I. Shitanda, Y. Hoshi, M. Itagaki, T. Tojo, M. Yuasa, *Carbon* **2021**, *173*, 395.
[71] M. Ficek, M. Cieślik, M. Janik, M. Brodowski, M. Sawczak, R. Bogdanowicz, J. Ryl, *Microchim. Acta* **2023**, *190*, 410.
[72] X. Zhang, S. Wei, C. Lei, J. wei, B. Lu, Y. Ding, C. Zhu, *Appl. Surf. Sci.* **2011**, *257*, 5185.
[73] A. Perl, D. N. Reinhoudt, J. Huskens, *Adv. Mater.* **2009**, *21*, 2257.
[74] A. Ruiz, S. Chen, C. S. Microcontact, *Soft Matter* **2007**, *3*, 168.
[75] T. Kaufmann, B. J. S. Ravoo, *Polym. Chem.* **2010**, *1*, 371.
[76] H. Zhuang, B. Song, T. Staedler, X. Jiang, *Langmuir* **2011**, *27*, 11981.
[77] B. Yan, Z. Zhao, X. Wu, H. Li, D. Liu, *Diam. Relat. Mater.* **2024**, *145*, 111078.
[78] W. Tong, K. Fox, K. Ganesan, S. Prawer, *Proc. Technol* **2015**, *20*, 206.
[79] M. A. Shah, D. G. Lee, B. Y. Lee, S. Hur, *IEEE Access* **2021**, *9*, 140079.
[80] K. Zub, S. Hoeppener, U. S. Schubert, *Adv. Mater.* **2022**, *34*, 2105015.
[81] Y.-C. Chen, Y. Tzeng, A.-J. Cheng, R. Dean, M. Park, B. M. Wilamowski, *Diam. Relat. Mater.* **2009**, *18*, 146.
[82] A. F. Sartori, P. Belardinelli, R. J. Dolleman, P. G. Steeneken, M. K. Ghatkesar, J. G. Buijnsters, *Small* **2019**, *15*, 1803774.
[83] D. Lohse, *Annu. Rev. Fluid Mech.* **2022**, *54*, 349.
[84] N. A. Fox, M. J. Youh, J. W. Steeds, W. N. Wang, *J. Appl. Phys.* **2000**, *87*, 8187.
[85] Y.-C. Chen, Y. Tzeng, A. Davray, A.-J. Cheng, R. Ramadoss, M. Park, *Diam. Relat. Mater.* **2008**, *17*, 722.
[86] P. Kulha, J. Kroutil, A. Laposa, V. Procházka, M. Husák, *J. Electr. Eng.* **2016**, *67*, 61.
[87] A. Laposa, J. Kroutil, M. Davydova, A. Taylor, J. Voves, L. Klimsa, J. Kopecek, M. Husak, *IEEE Sens. J.* **2020**, *20*, 1158.
[88] Z. Liu, S. Baluchová, B. Brocken, E. Ahmed, P. Pobedinskas, K. Haenen, J. G. Buijnsters, *ACS Appl. Mater. Interfaces* **2023**, *15*, 39915.
[89] J. Nahlik, A. Laposa, J. Voves, J. Kroutil, J. Drahokoupil, M. Davydova, *IEEE Sens. J.* **2019**, *19*, 5587.
[90] Z. Xu, L. Wang, X. Huan, H. Lee, J. Yang, Z. Zhou, M. Chen, S. Hu, Y. Liu, S.-P. Feng, T. Zhang, F. Xu, Z. Chu, J. T. Kim, *Adv. Sci.* **2022**, *9*, 2103598.
[91] Z. Chu, J. Peng, W. Jin, *Sens. Actuator B-Chem.* **2017**, *243*, 919.
[92] A. P. Quist, E. Pavlovic, S. Oscarsson, *Anal. Bioanal. Chem.* **2005**, *381*, 591.
[93] H. A. G. R. Centres, Inkjet Printing Process for Kesterite Solar Cells **2015**. Available at: https://phys.org/news/2015-05-inkjet-kesterite-solar-cells.html (accessed: August 2025).

© 2025 The Author(s). Advanced Materials Technologies published by Wiley-VCH GmbH

2365709x, 2025, 22, Downloaded from https://advanced.onlinelibrary.wiley.com/doi/10.1002/admt.202501111, Wiley Online Library on [19/11/2025]. See the Terms and Conditions (https://onlinelibrary.wiley.com/terms-and-conditions) on Wiley Online Library for rules of use; OA articles are governed by the applicable Creative Commons License

[94] S. C. Ligon, R. Liska, J. Stampfl, M. Gurr, R. Mülhaupt, *Chem. Rev.* **2017**, *117*, 10212.
[95] J.-Y. Lee, J. An, C. K. Chua, *Appl. Mater. Today* **2017**, *7*, 120.
[96] K. Rajan, M. Samykano, K. Kadirgama, W. S. W. Harun, M. M. Rahman, *J. Adv. Manuf. Technol.* **2022**, *120*, 1531.
[97] B. Liu, Y. Wang, Z. Lin, T. Zhang, *Mater. Lett.* **2020**, *263*, 127252.
[98] U. Kalsoom, S. Waheed, B. Paull, *ACS Appl. Mater. Interfaces* **2020**, *12*, 4962.
[99] R. Chaudhary, P. Fabbri, E. Leoni, F. Mazzanti, R. Akbari, C. Antonini, *Prog. Addit. Manuf.* **2023**, *8*, 331.
[100] J. Huang, Q. Qin, J. A. R. S. Wang, *Processes* **2020**, *8*, 1138.
[101] W. Han, L. Kong, M. Xu, *Int. J. Extreme Manuf.* **2022**, *4*, 042002.
[102] E. M. Sefene, *J. Manuf. Syst.* **2022**, *63*, 250.
[103] M. Ghasempour-Mouziraji, J. Lagarinhos, D. Afonso, *Opt. Laser Technol.* **2024**, *170*, 110226.
[104] U. Kalsoom, A. Peristyy, P. N. Nesterenko, B. Paull, *RSC Adv.* **2016**, *6*, 38140.
[105] H. Khakbaz, S. Sayyar, S. Beirne, M. Heitzmann, P. C. Innis, *Macromol. Rapid Commun.* **2023**, *44*, 2300335.
[106] S. Waheed, J. M. Cabot, P. Smejkal, S. Farajikhah, S. Sayyar, P. C. Innis, S. Beirne, G. Barnsley, T. W. Lewis, M. C. Breadmore, B. Paull, *ACS Appl. Mater. Interfaces* **2019**, *11*, 4353.
[107] Z. Chen, K. Li, P. Han, Y. Pan, G. Bai, Z. Xia, N. Xiao, P. Wang, *Sci. Rep.* **2024**, *14*, 30054.
[108] J. Wu, Y. Wang, Z. Wang, S. Zhang, X. Zeng, X. Kong, W. Gao, T. Chen, Y. Liu, J. Bin, *Int. J. Refract. Met. Hard Mater.* **2025**, *128*, 107014.
[109] J. Wu, Q. Zhang, Y. Li, S. Zhang, X. Kong, L. Rong, Y. Xiao, H. Li, Z. Ding, *Diam. Relat. Mater.* **2024**, *150*, 111760.
[110] J. Wu, X. Zhao, Q. Zhang, S. Zhang, X. Kong, L. Rong, Y. Li, W. Gao, Z. Xu, *Sci. Rep.* **2024**, *14*, 28937.
[111] Z. Yang, J. Hu, K. Li, A. Liu, S. Liu, *Adv. Eng. Mater.* **2018**, *20*, 1700747.
[112] A. T. Sidambe, *Materials* **2014**, *7*, 8168.
[113] T. Billiet, M. Vandenhaute, J. Schelfhout, S. Van Vlierberghe, P. Dubruel, *Biomaterials* **2012**, *33*, 6020.
[114] C. Doñate-Buendia, R. Streubel, P. Kürnsteiner, M. B. Wilms, F. Stern, J. Tenkamp, E. Bruder, S. Barcikowski, B. Gault, K. Durst, J. H. Schleifenbaum, F. Walther, B. Gökce, *Proc. CIRP* **2020**, *94*, 41.
[115] P. Verding, P. Pobedinskas, R. M. Joy, E. Ahmed, Z. Remes, R. S. N. Kumar, S. Baron, M. Höfer, V. Sittinger, M. Nesládek, K. Haenen, W. Deferme, *Surf. Coat. Technol.* **2023**, *459*, 129391.
[116] P. Verding, R. Mary Joy, D. Reenaers, R. S. N. Kumar, R. Rouzbahani, E. Jeunen, S. Thomas, D. Desta, H.-G. Boyen, P. Pobedinskas, K. Haenen, W. Deferme, *ACS Appl. Mater. Interfaces* **2024**, *16*, 1719.
[117] A. C. Taylor, R. Edgington, R. B. Jackman, *ACS Appl. Mater. Interfaces* **2015**, *7*, 6490.
[118] J. Kozak, K. Tyszczuk-Rotko, M. Wójciak, I. Sowa, M. Rotko, *Materials* **2021**, *14*, 4231.
[119] L. R. G. Silva, J. G. A. Rodrigues, L. S. de, M. Vasconcellos, E. S. Ribeiro, E. D'Elia, Q. de, R. Ferreira, *Ionics* **2022**, *28*, 4833.
[120] J. Kozak, K. Tyszczuk-Rotko, A. Keller, M. Wójciak, I. Sowa, *Materials* **2023**, *16*, 6826.
[121] S. Đurđić, F. Vlahović, M. Markićević, J. Mutić, D. Manojlović, V. Stanković, Ľ. Švorc, D. Stanković, *Chemosensors* **2023**, *11*, 15.
[122] R. Šelešovská, T. Navrátil, V. Hrdlička, P. Michniak, M. Hatala, M. Vojs, M. Marton, O. Matvieiev, L. Janíková, J. Chýlková, *Electrochim. Acta* **2022**, *403*, 139642.
[123] O. Matvieiev, R. Selesovská, M. Vojs, M. Marton, P. Michniak, V. Hrdlicka, M. Hatala, L. Janíková, J. Chýlková, J. Skopalová, P. Cankar, T. Navrátil, *Biosensors* **2022**, *12*, 241.
[124] O. Matvieiev, R. Šelešovská, R. Sokolová, R. Jerga, J. Skopalová, P. Barták, J. Chýlková, M. Vojs, *Sens. Actuator B-Chem.* **2023**, *397*, 134700.
[125] O. Matvieiev, R. Šelešovská, M. Marton, M. Hatala, R. Metelka, M. Weis, M. Vojs, *Sci. Rep.* **2023**, *13*, 21525.
[126] P. Kelíšková, O. Matvieiev, E. Jiroušková, R. Sokolová, L. Janíková, M. Behúl, R. Šelešovská, *Talanta* **2025**, *281*, 126809.
[127] Y. Wang, B. Sun, *Appl. Phys. Lett.* **2024**, *125*, 042202.
[128] R. Chen, Q. Lian, D. Li, X. He, S. Wang, J. Zhuang, *Ceram. Int.* **2021**, *47*, 14009.
[129] M. Shekhar, S. K. S. Yadav, *Mater. Today Proc.* **2020**, *22*, 3126.
[130] J. Konstanty, *Materials Science Forum*, Trans Tech Publications, Ltd, Switzerland **2007**, *534–536*, pp. 1121.
[131] T. J. Lu, J. Ke, Y. Lan, Z. H. Song, J. Zhang, S. Tang, J. Su, H. R. Dai, X. X. Wu, *J. Gemmol.* **2019**, *36*, 748.
[132] J. Konstanty, *Arch. Metall. Mater.* **2021**, *66*, 593.
[133] J. Wu, S. Zhang, L. Liu, F. Qu, H. Zhou, Z. Su, *Int. J. Refract. Met. Hard Mater.* **2020**, *89*, 105212.
[134] T. He, S. Zhang, X. Kong, J. Wu, L.-l. Liu, D. Wu, Z. Su, *J. Alloys Compd.* **2023**, *931*, 167492.
[135] X. Kong, Y. Wang, J. Wu, D. Wu, S. Zhang, L. Rong, *Int. J. Refract. Met. Hard Mater.* **2024**, *123*, 106775.
[136] N. Kraiem, N. Tessier-Doyen, A. Mao, G. Ji, F. Wang, E. Loubère, H. Dong, Q. Zhu, B. Cui, J.-F. Silvain, Y. F. Lu, *Adv. Eng. Mater.* **2025**, *27*, 2402366.
[137] C. Tian, Y. Tang, Y. Zou, Y. Wan, X. Li, *Int. J. Refract. Met. Hard Mater.* **2024**, *124*, 106821.
[138] L. Chen, R. Wilson, G. de Looze, K. Yang, A. Seeber, *Mater. Sci. Eng. A* **2023**, *884*, 145579.
[139] X. Fang, Z. Yang, S. Tan, L. Duan, *Crystals* **2020**, *10*, 596.
[140] R. Rahmani, M. Antonov, L. Kollo, *Adv. Tribol.* **2019**, *2019*, 5415897.
[141] R. Rahmani, M. Antonov, L. Kollo, *Adv. Mater. Sci. Eng.* **2019**, *2019*, 4210762.
[142] R. Rahmani, M. Brojan, M. Antonov, K. G. Prashanth, *Int. J. Refract. Met. Hard Mater.* **2020**, *88*, 105192.
[143] X. Kong, J. Wu, D. Wu, L. Rong, S. Zhang, *Addit. Manuf.* **2024**, *91*, 104325.
[144] X. Meng, W. Yang, X. Deng, *Diam. Relat. Mater.* **2021**, *120*, 108715.
[145] W. Yang, X. Meng, P. Ni, Z. Zhao, X. Deng, S. Wu, Z. Qu, F. Jin, *Ceram. Int.* **2023**, *49*, 16891.
[146] H. Shao, K. Zhao, T. Lin, J. Xu, *Mater. Today Commun.* **2024**, *39*, 108678.
[147] J. Tang, H. Zhang, H. Chang, X. Guo, C. Wang, Y. Wei, Z. Huang, Y. Yang, *J. Eur. Ceram.* **2023**, *43*, 5436.
[148] D. Tang, H. Tang, *Addit. Manuf.* **2022**, *56*, 102898.
[149] J. S. L. Fong, M. A. Booth, A. Rifai, K. Fox, A. Gelmi, *Adv. Healthcare Mater.* **2021**, *10*, 2100007.
[150] N. Priyadarshni, R. Singh, M. K. N. Mishra, *Cancer Lett* **2024**, *587*, 216710.
[151] E. K. Chow, X.-Q. Zhang, M. Chen, R. Lam, E. Robinson, H. Huang, D. Schaffer, E. Osawa, A. Goga, *Sci. Transl. Med.* **2011**, *3*, 73ra21.
[152] S. Szunerits, A. Barras, R. Boukherroub, *Int. J. Environ. Res. Public Health* **2016**, *13*, 413.
[153] K. Turcheniuk, V. N. Mochalin, *Nanotechnology* **2017**, *28*, 252001.
[154] M. Angjellari, E. Tamburri, L. Montaina, M. Natali, D. Passeri, M. Rossi, M. L. Terranova, *Mater. Des.* **2017**, *119*, 12.
[155] K. Fox, N. Mani, A. Rifai, P. Reineck, A. Jones, P. A. Tran, A. Ramezannejad, M. Brandt, B. C. Gibson, A. D. Greentree, N. Tran, *ACS Appl. Bio Mater.* **2020**, *3*, 29.
[156] N. Mani, A. Ahnood, D. Peng, W. Tong, M. Booth, A. Jones, B. Murdoch, N. Tran, S. Houshyar, K. Fox, *ACS Appl. Mater. Interfaces* **2021**, *13*, 31474.
[157] N. Mani, N. Tran, A. Jones, A. Mirabedini, S. Houshyar, K. Fox, *Rapid Prototyp. J.* **2024**, *30*, 1989.
[158] K. Ganesan, D. J. Garrett, A. Ahnood, M. N. Shivdasani, W. Tong, A. M. Turnley, K. Fox, H. Meffin, S. Prawer, *Biomaterials* **2014**, *35*, 908.

© 2025 The Author(s). Advanced Materials Technologies published by Wiley-VCH GmbH

2365709x, 2025, 22, Downloaded from https://advanced.onlinelibrary.wiley.com/doi/10.1002/admt.202501111, Wiley Online Library on [19/11/2025]. See the Terms and Conditions (https://onlinelibrary.wiley.com/terms-and-conditions) on Wiley Online Library for rules of use; OA articles are governed by the applicable Creative Commons License

[159] U. Mangal, Y. J. Min, J.-Y. Seo, D.-E. Kim, J.-Y. Cha, K.-J. Lee, J.-S. Kwon, S.-H. Choi, *J. Mech. Behav. Biomed. Mater.* **2020**, *110*, 103992.
[160] U. Mangal, J.-Y. Seo, J. Yu, J.-S. Kwon, S.-H. Choi, *Nanomaterials* **2020**, *10*, 827.
[161] K. U. Laszczyk, *Micromachines* **2020**, *11*, 260.
[162] E. Kowalewska, M. Ficek, K. Formela, A. Zieliński, S. Kunuku, M. Sawczak, R. Bogdanowicz, *Nanomaterials* **2022**, *12*, 2604.
[163] J. O. Orwa, A. D. Greentree, I. Aharonovich, A. D. C. Alves, J. Van Donkelaar, A. Stacey, S. Prawer, *J. Lumin.* **2010**, *130*, 1646.
[164] O. A. Shenderova, A. I. Shames, N. A. Nunn, M. D. Torelli, I. Vlasov, A. Zaitsev, *J. Vac. Sci. Technol. B:Nanotechnol.* **2019**, *37*, 030802.
[165] B. T. Flinn, V. Radu, M. W. Fay, A. J. Tyler, J. Pitcairn, M. J. Cliffe, B. L. Weare, C. T. Stoppiello, M. L. Mather, A. N. Khlobystov, *Nanoscale Adv* **2023**, *5*, 6423.



Simona Baluchová is an assistant professor in the Department of Analytical Chemistry, Faculty of Science, Charles University, Czech Republic. After earning her Ph.D. in Analytical Chemistry (cum laude, Charles University, 2021), she joined Delft University of Technology, The Netherlands, as a postdoctoral fellow, where she secured a grant from the Dutch Research Council to pioneer printable diamond electrodes. She is currently the holder of a Primus project grant, supporting top young researchers at Charles University. Her research focuses on the development of electrochemical sensors and novel electrode materials, including those based on conductive diamond, and applying additive manufacturing in electrochemistry.



Josephus G. Buijnsters is an associate professor in the section Micro and Nano Engineering of Department of Precision and Microsystems Engineering at Delft University of Technology, The Netherlands. Dr. Buijnsters has co-authored over 90 peer-reviewed publications and specialized in surface-engineered synthetic diamond. His current research focuses on conductive diamond for energy technology, wastewater treatment, and sensing. He received a Ph.D. in Applied Physics and a M.Sc. Degree in Chemistry from Radboud University, Nijmegen, The Netherlands.

© 2025 The Author(s). Advanced Materials Technologies published by Wiley-VCH GmbH

2365709x, 2025, 22, Downloaded from https://advanced.onlinelibrary.wiley.com/doi/10.1002/admt.202501111, Wiley Online Library on [19/11/2025]. See the Terms and Conditions (https://onlinelibrary.wiley.com/terms-and-conditions) on Wiley Online Library for rules of use; OA articles are governed by the applicable Creative Commons License